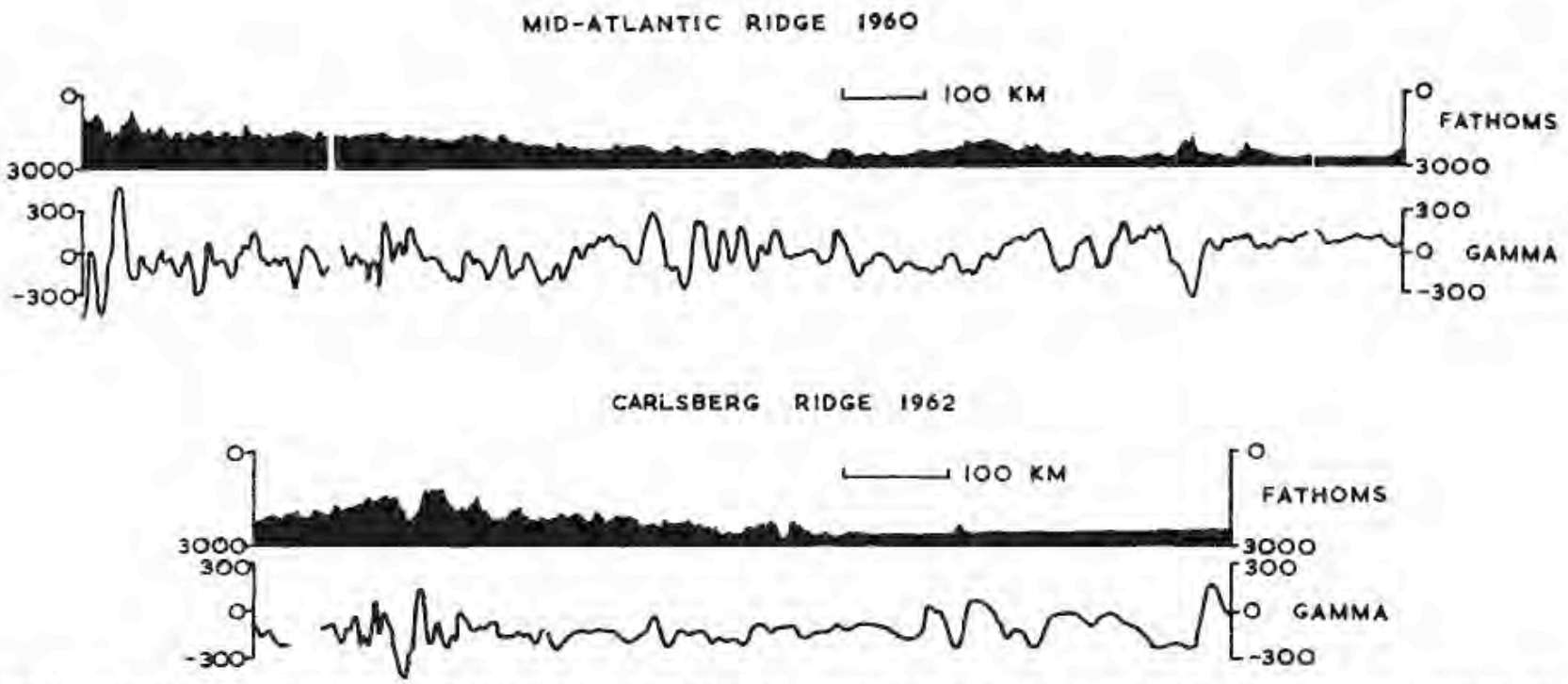

Fig. 1. Profiles showing bathymetry and the associated total magnetic field anomaly observed on crossing the North Atlantic and the northwest Indian Oceans. Upper profile from 45° 17′ N, 28° 27′ W. to 45° 19′ N. 11° 29′ W. Lower profile from 30° 5′ N. 61° 57′ E. to 10° 10′ N. 66° 27′ E.

Vine and Mathews 1963

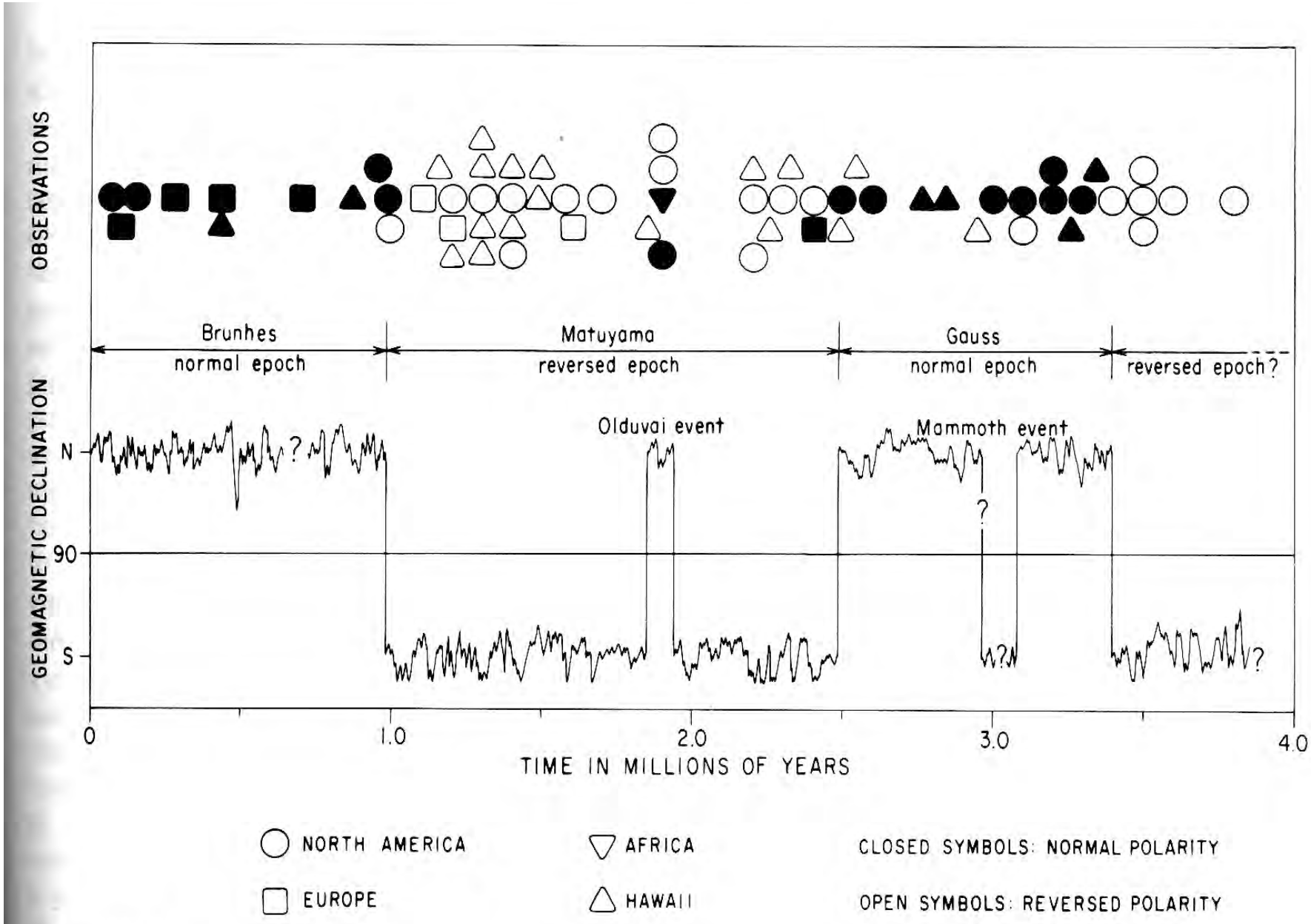

Figure 16-3
Magnetic polarities of 64 volcanic rock and their potassium-argon ages (see footnote 1, page 175). Geomagnetic declination for moderate latitudes is indicated schematically

Cox et al 1964

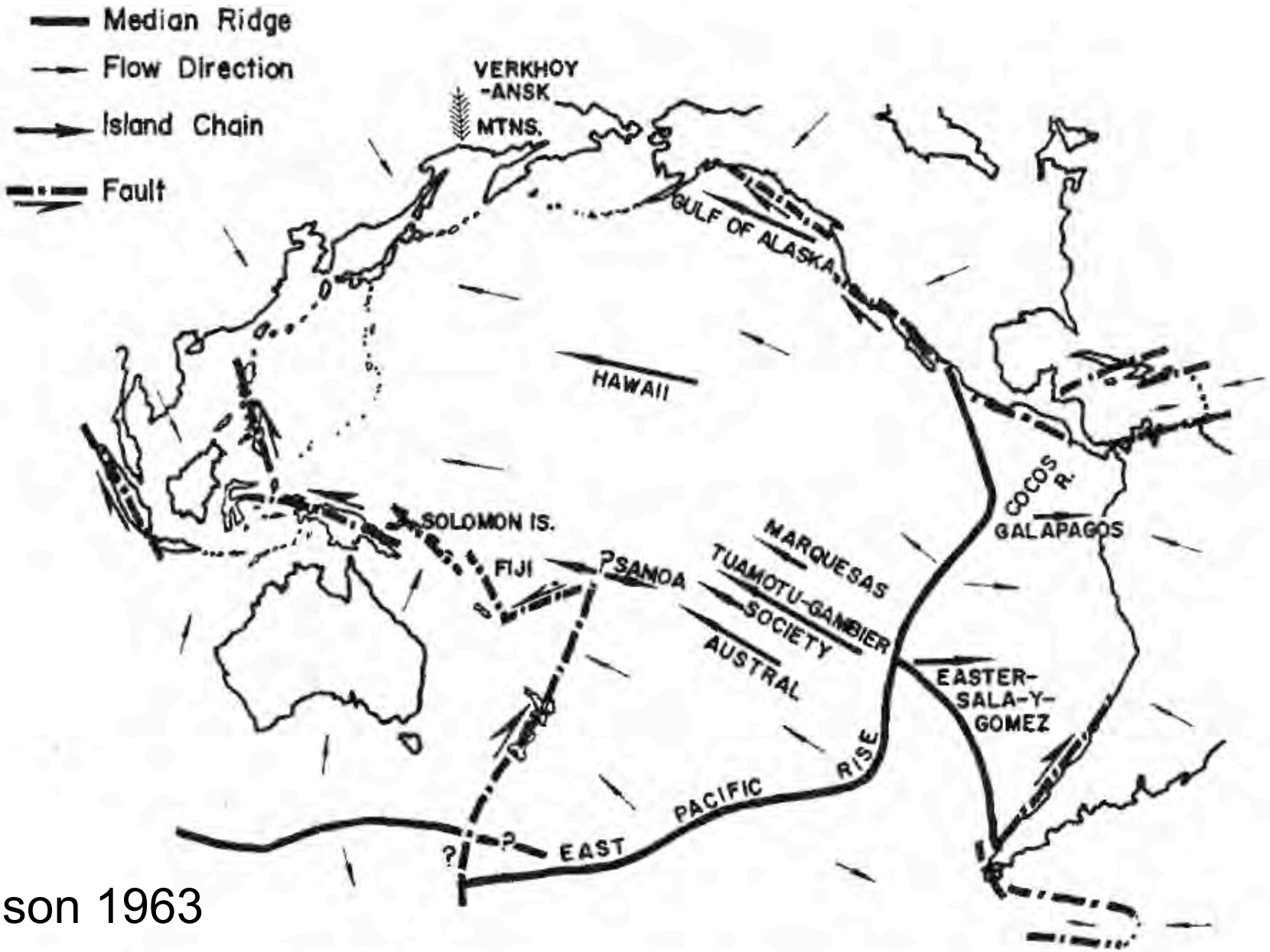

Wilson 1963

FIG. 1. Sketch of Pacific Ocean. Heavy arrows show nine linear chains of islands and seamounts which increase in age in direction of arrow. Single-headed arrows show direction of motion, where known, along large transcurrent faults. Small arrows show postulated direction of flow away from median ridges.

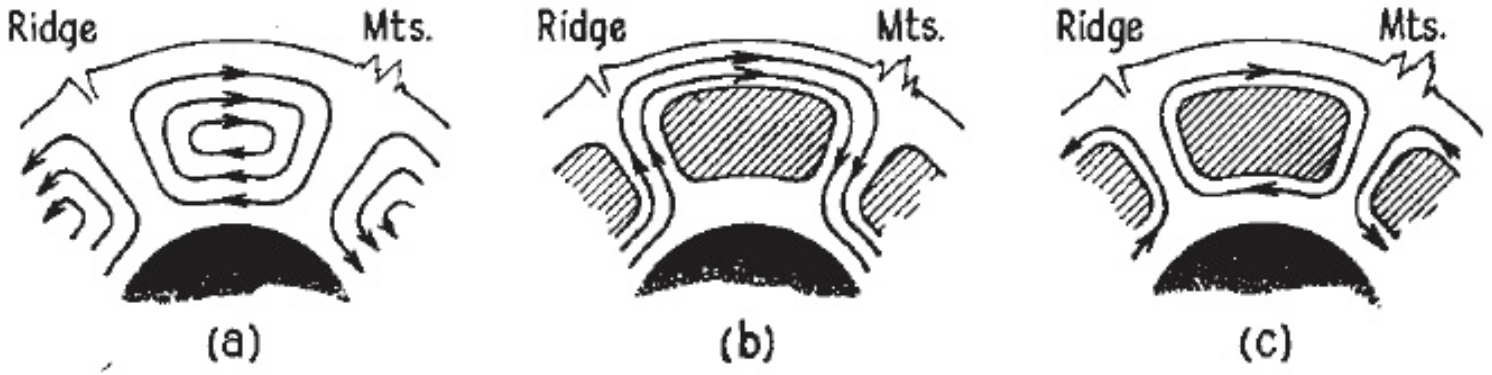

FIG. 2. Three possible modes of convection in the Earth's mantle.

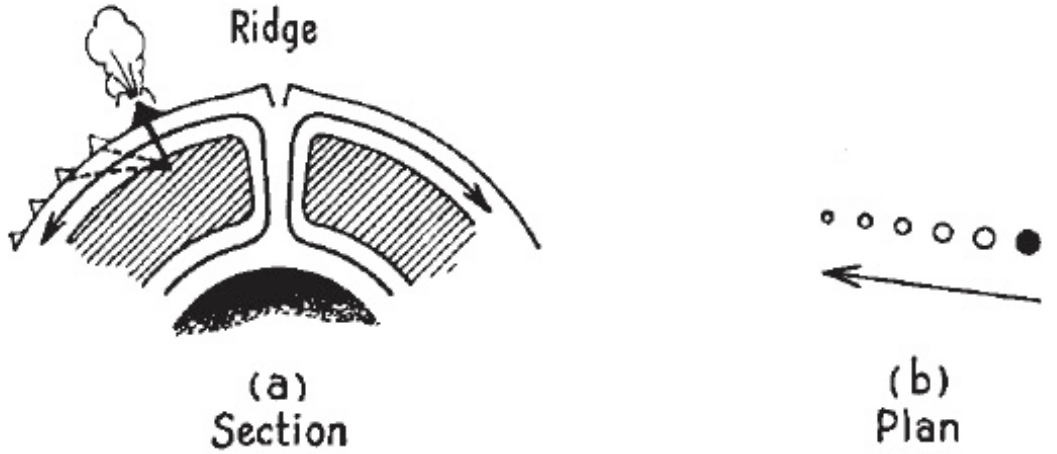

Wilson 1963

FIG. 5. Diagram to illustrate that if lava is generated in the stable core of a convection cell, and the surface is carried by the jet stream, then one source can give rise to a chain of extinct volcanoes even if the source is not over a rising current. This is proposed as a possible origin of the Hawaiian chain of islands.

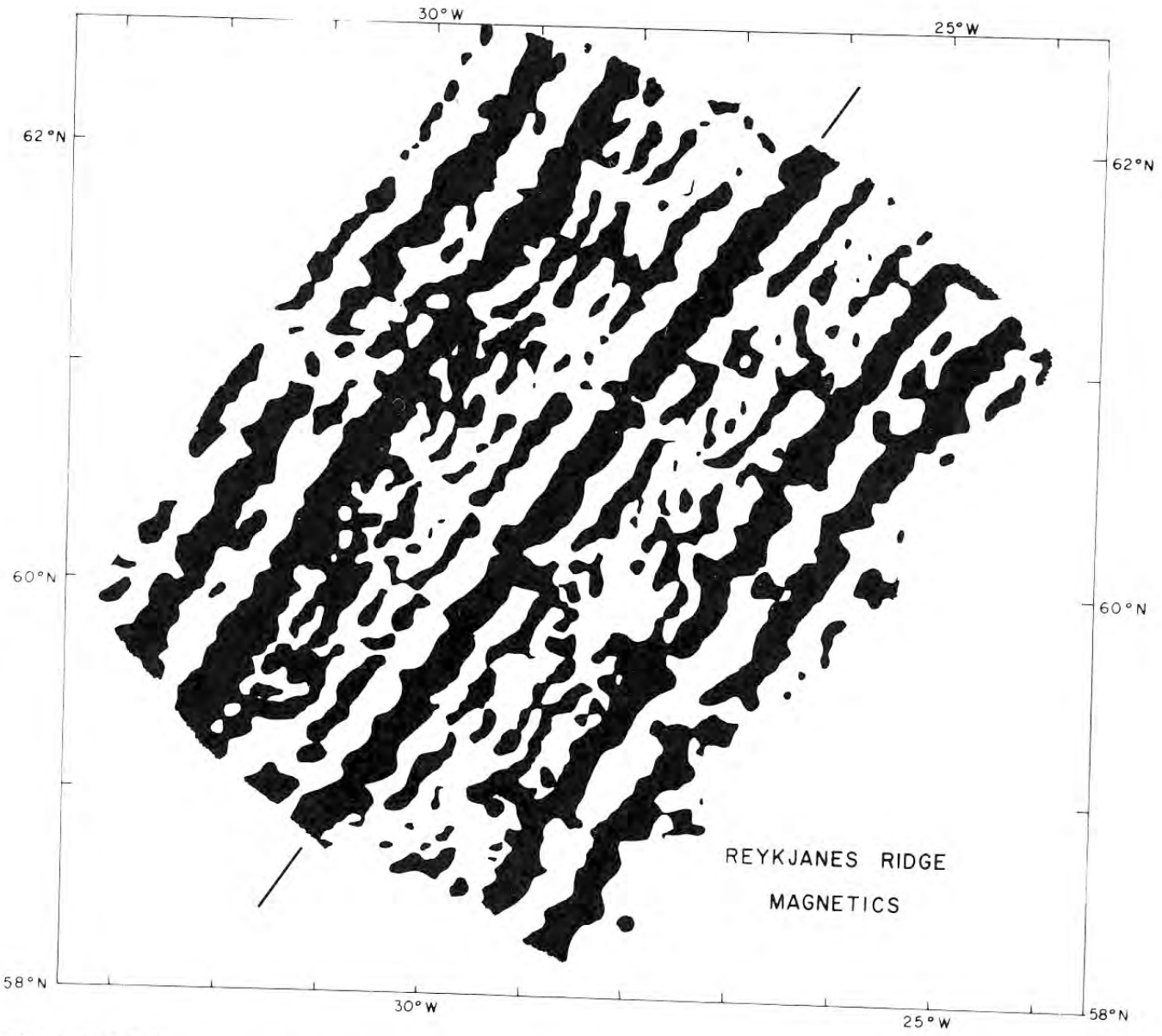

Figure 24-3
Summary diagram of the magnetic anomalies observed over Reykjanes Ridge (see Figure 24-2). Straight lines indicate the axis of the ridge and the central positive anomaly (Heirtzler et al., 1966)

Vine 1966

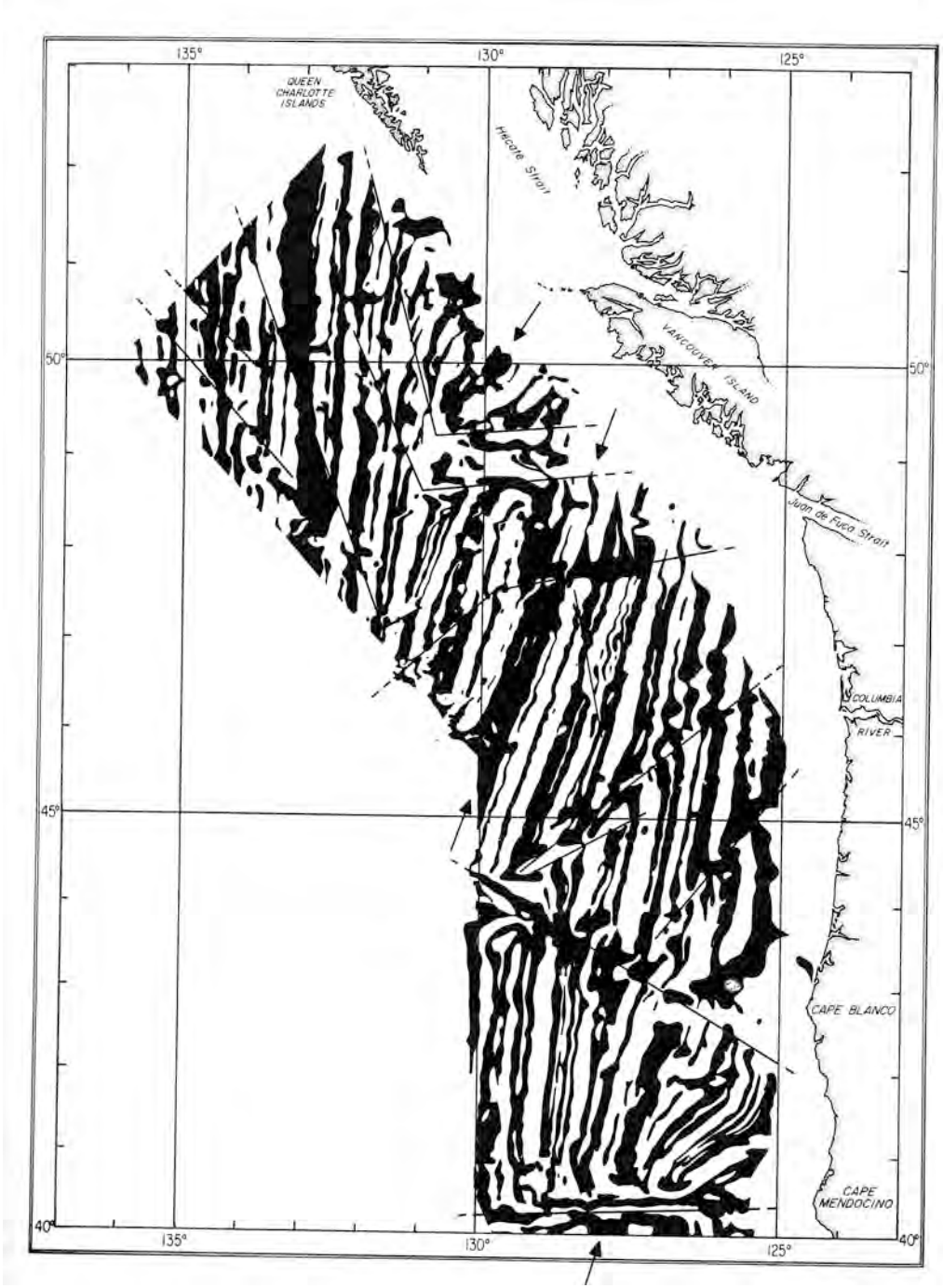
135°
130°
125°
QUEEN CHARLOTTE ISLANDS
Hecate Strait
VANCOUVER ISLAND
50°
Juan de Fuca Strait
COLUMBIA RIVER
45°
CAPE BLANCO
CAPE MENDOCINO
40°

Vine 1966

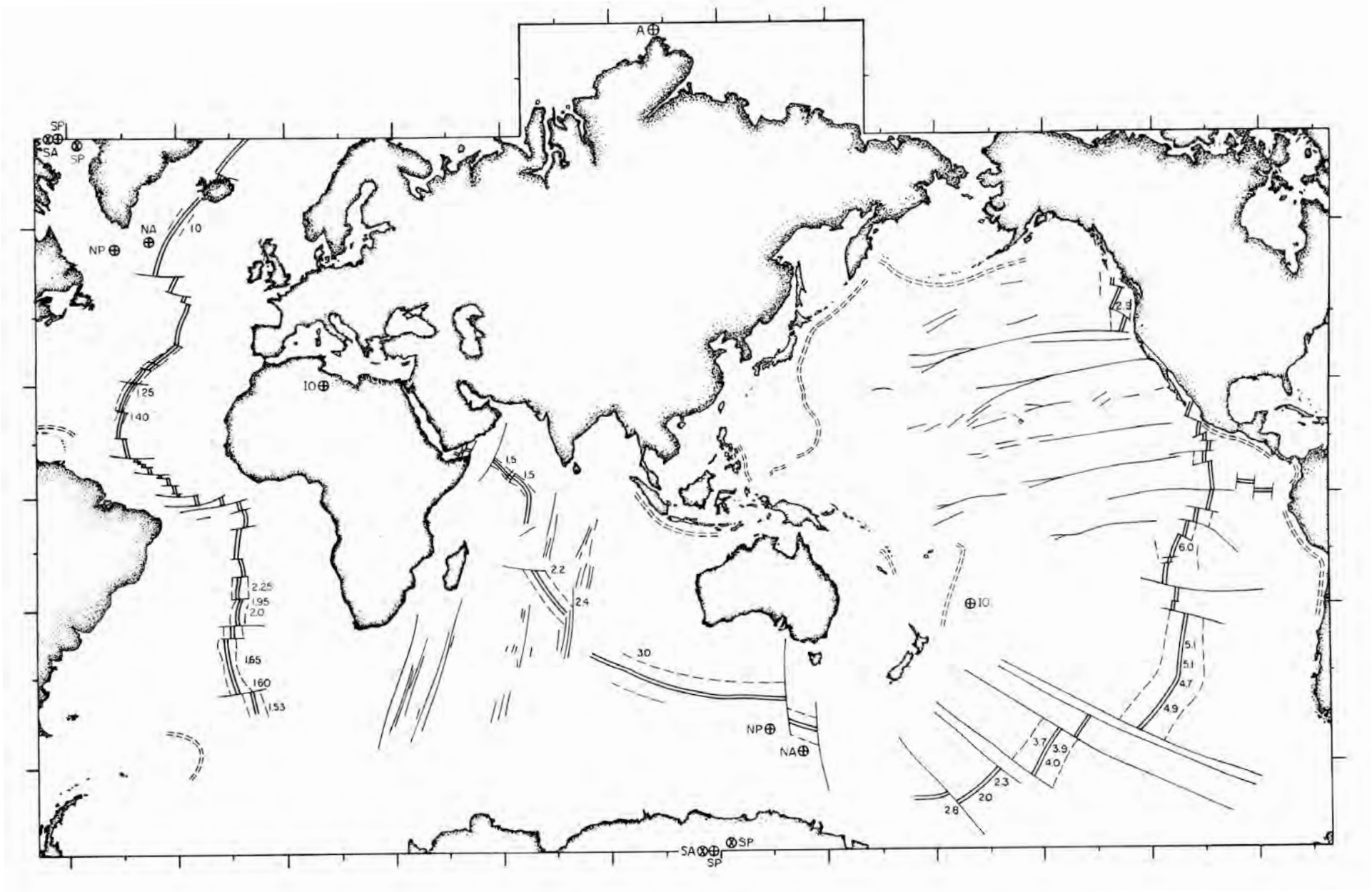

Le Pechon 1968

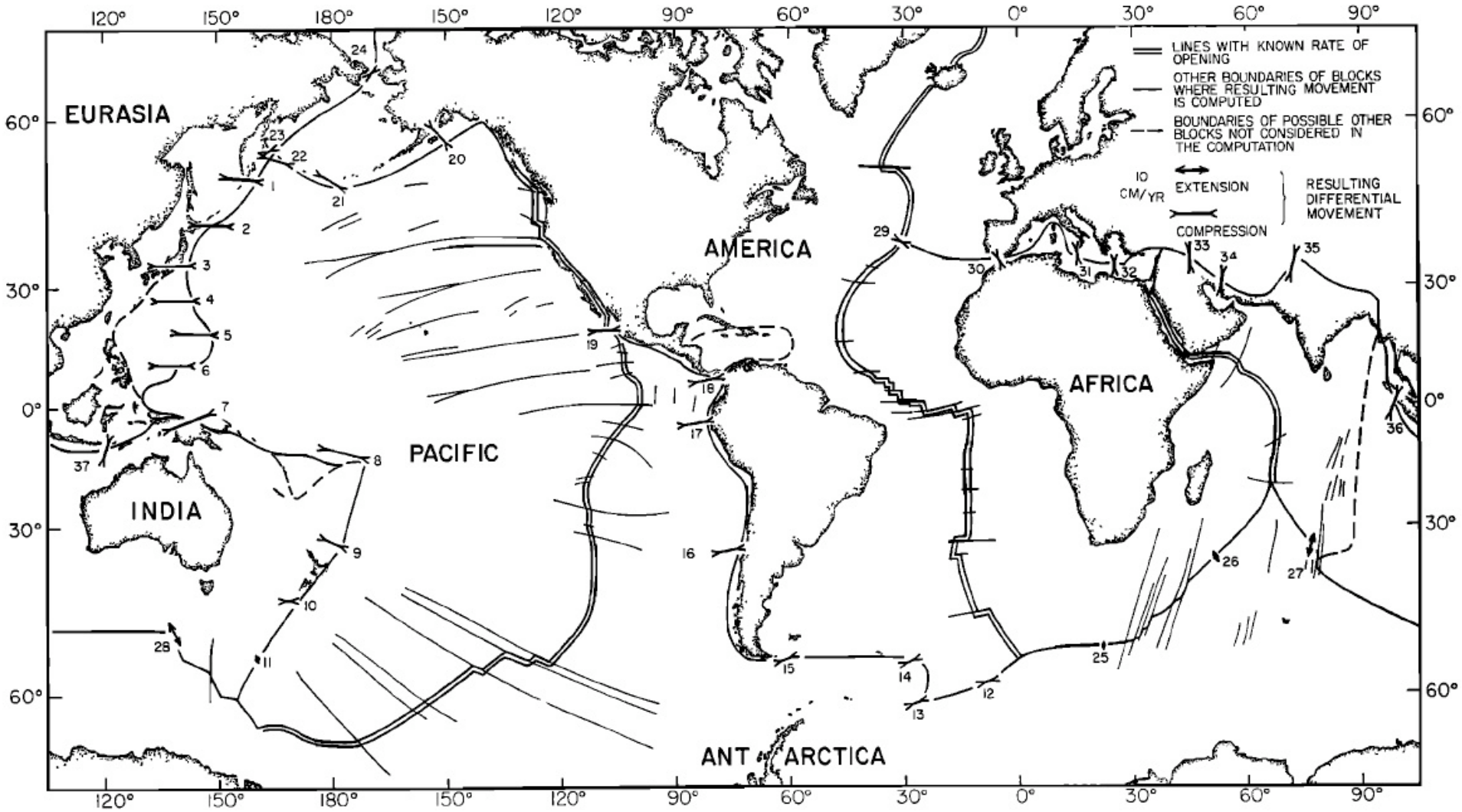

Fig. 6. The locations of the boundaries of the six blocks used in the computations. The numbers next to the vectors of differential movement refer to Table 5. Note that the boundaries where the rate of shortening or slippage exceeds about 2 cm/yr account for most of the world earthquake activity.

Le Pechon 1968

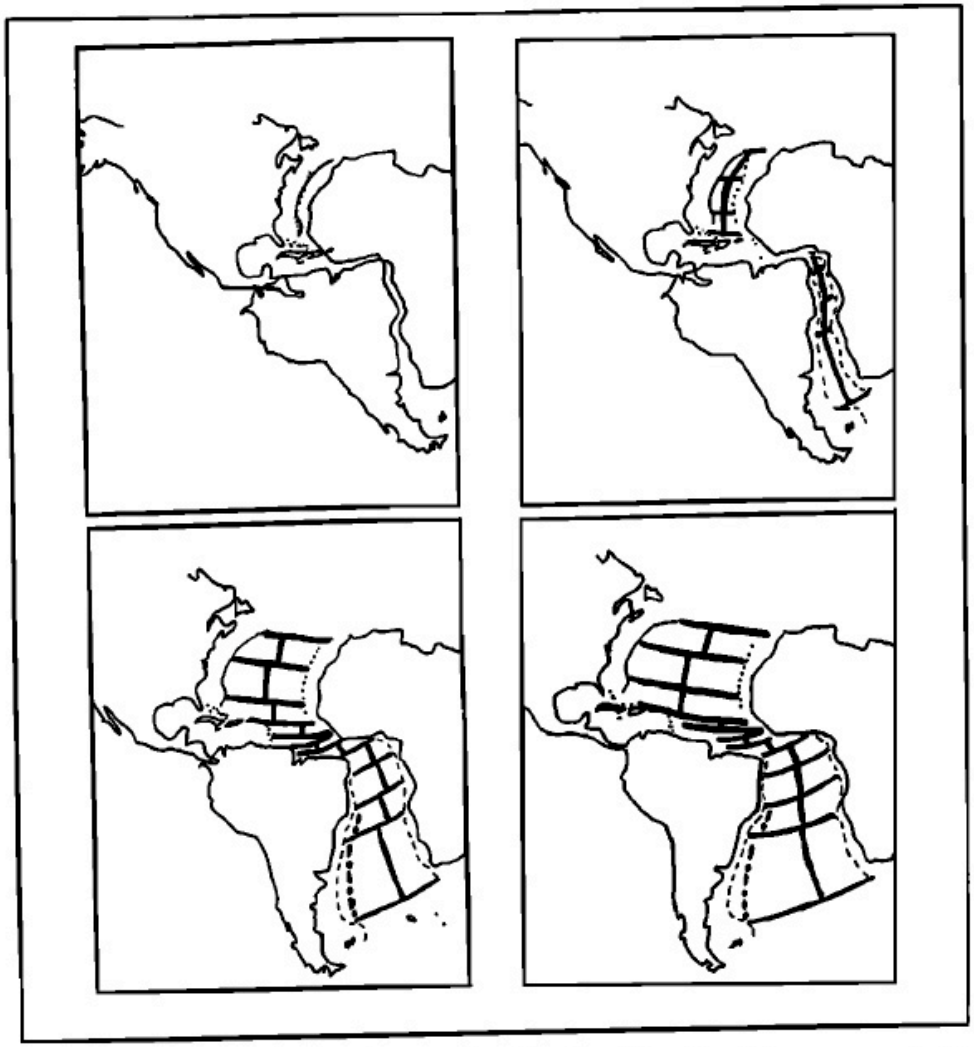

Fig. 10. The Mesozoic episode of spreading in the Atlantic. These reconstructions were obtained by assuming that North and South America parted simultaneously from Africa 120 m.y. ago (upper left) and reached the position corresponding to anomaly 31 (Figure 9) about 90 m.y. ago (lower right) after a single movement of rotation for each. The asymmetry of the ridge crest in the South Atlantic at the time of anomaly 31 is explained by a shift in the ridge crest positions in the Early Cretaceous. The fit is made to the 'quiet' magnetic zone boundaries in the North Atlantic and to the 500-fathom line in the South Atlantic [*Bullard et al.*, 1965]. See Table 7. The active ridge crests and fracture zones are represented by a thick continuous line, the abandoned ridge crest by a thick dash-dot line.

Le Pechon 1968

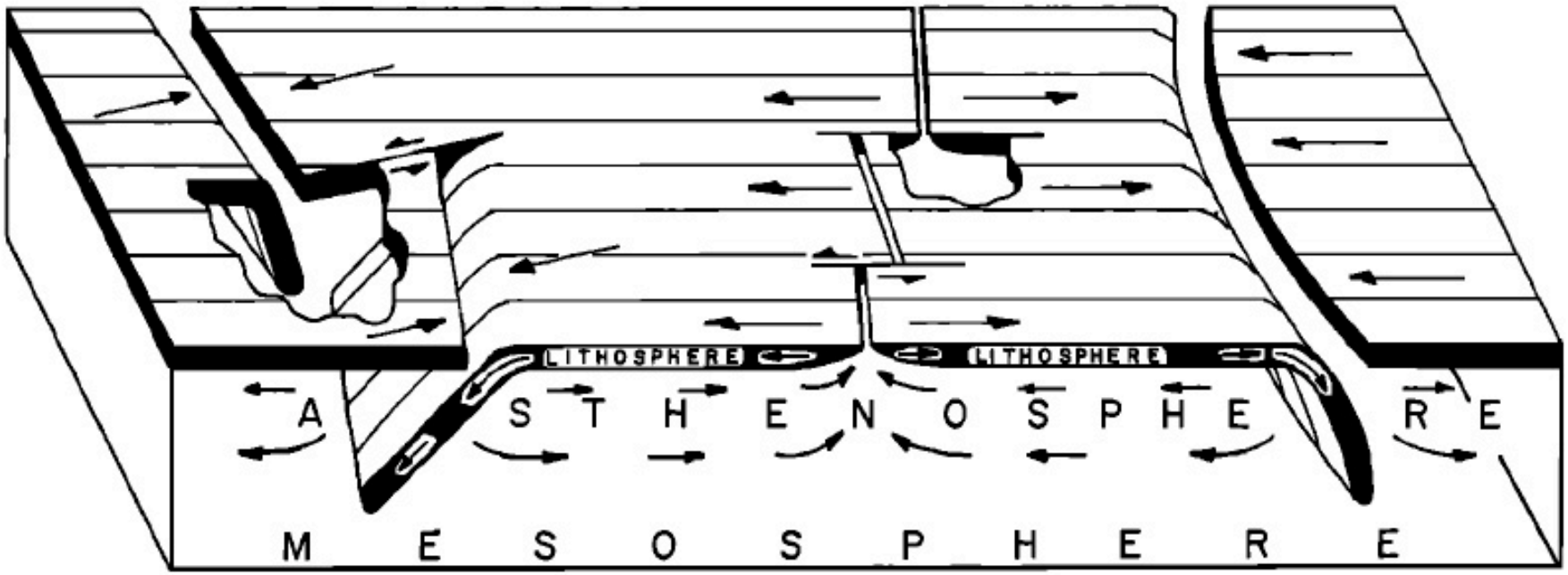

Fig. 1. Block diagram illustrating schematically the configurations and roles of the lithosphere, asthenosphere, and mesosphere in a version of the new global tectonics in which the lithosphere, a layer of strength, plays a key role. Arrows on lithosphere indicate relative movements of adjoining blocks. Arrows in asthenosphere represent possible compensating flow in response to downward movement of segments of lithosphere. One arc-to-arc transform fault appears at left between oppositely facing zones of convergence (island arcs), two ridge-to-ridge transform faults along ocean ridge at center, simple arc structure at right.

Isacks et al 1968

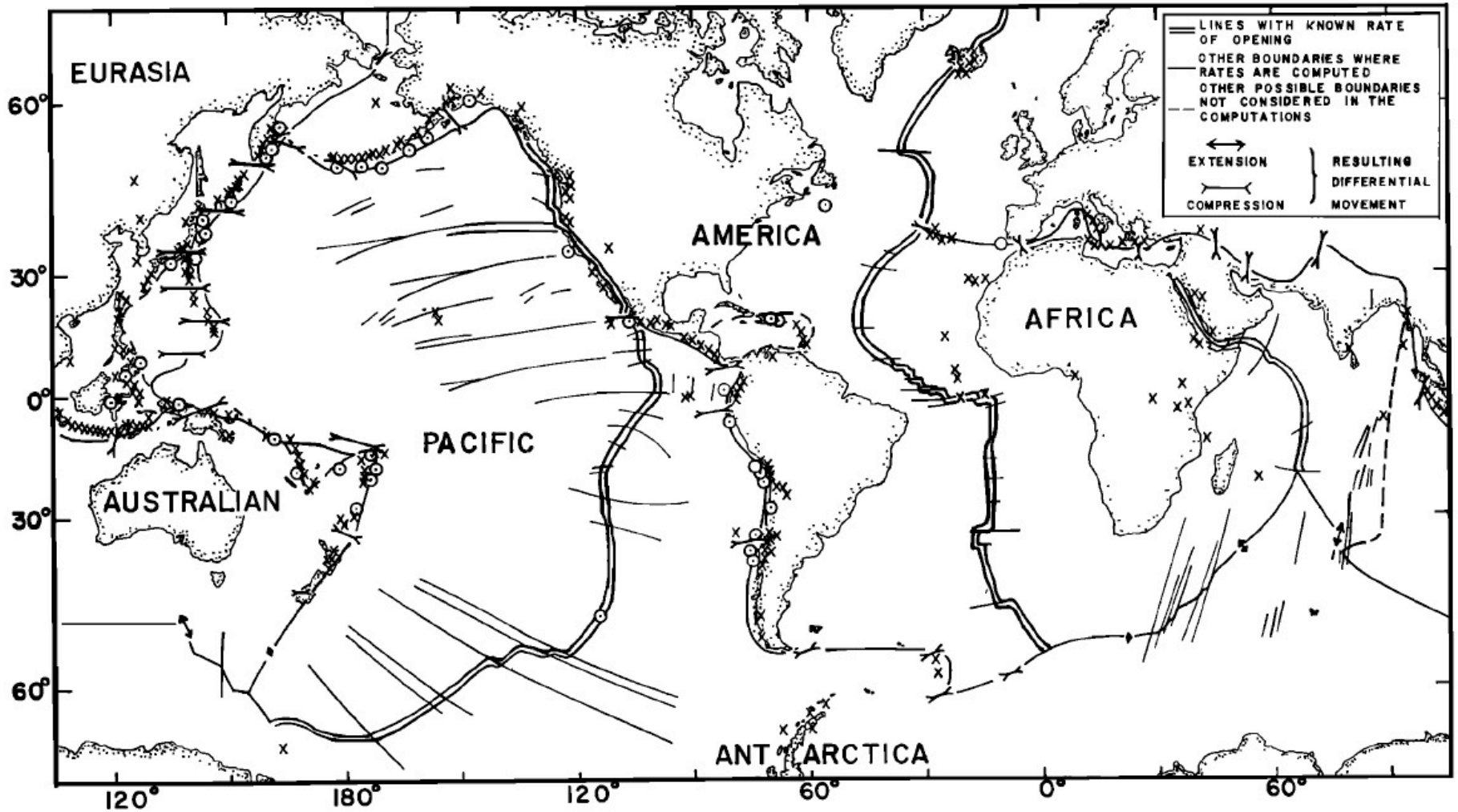

Fig. 2. Computed rates of compression and extension along boundaries of six lithospheric blocks [after *Le Pichon*, 1968]. Computed movements were derived from rates of spreading determined from magnetic data and from orientations of fracture zones along features indicated by double lines. The extensional and compressional symbols in the legend represent rates of 10 cm/yr; other similar symbols are scaled proportionally. Symbols appearing as diamonds represent small computed rates of extension for which the arrowheads coalesced. Historically active volcanoes [*Gutenberg and Richter*, 1954] are denoted by crosses. Open circles represent earthquakes that generated tsunamis (seismic sea waves) detected at distances of 1000 km or more from the source.

Isacks et al 1968

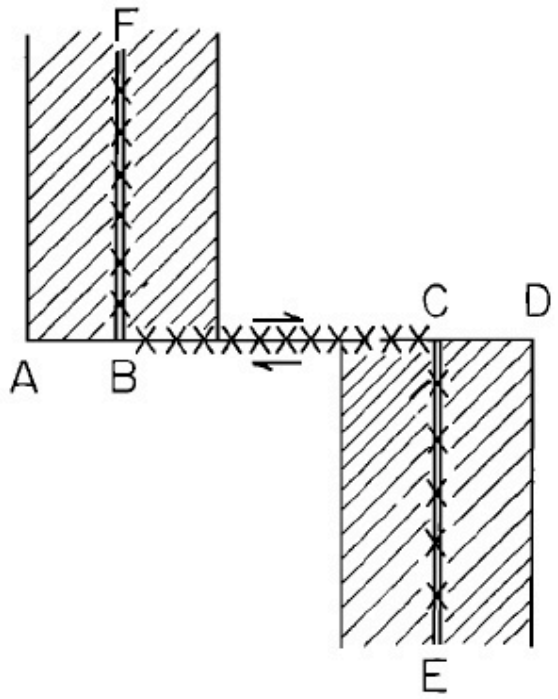

Fig. 4. An idealized model of sea-floor spreading and transform faulting of the ridge-ridge type. Hatching indicates new surface area created during a given period of sea-floor spreading along the active ridge crests BF and CE. Present seismicity (indicated by crosses) is confined to ridge crests and to segment BC of the fracture zone AD. Arrows denote sense of shear motion along active segment BC.

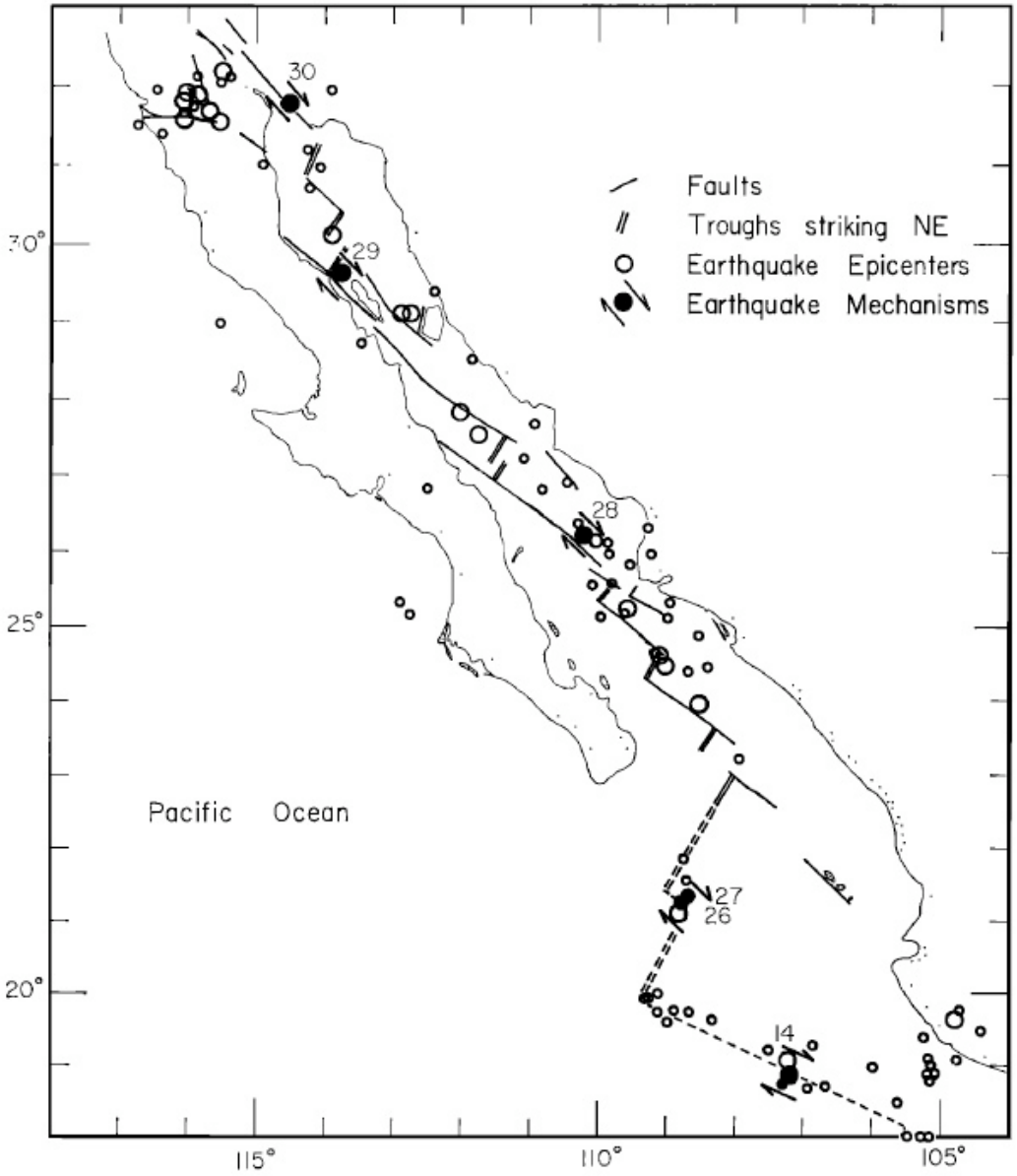

Fig. 6. Structural features of the Gulf of California [after *Sykes*, 1968]. Relocated epicenters of earthquakes for the period 1954 to 1962. Seismicity and focal mechanisms support the hypothesis of spreading by ocean-ridge–transform-fault mechanism.

Isacks et al 1968

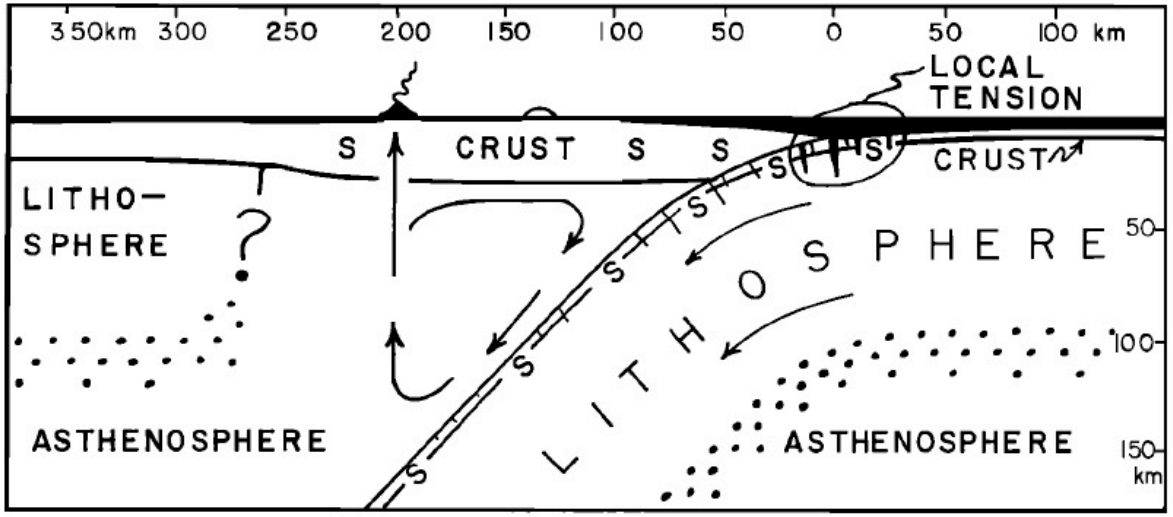

Fig. 7*a*.

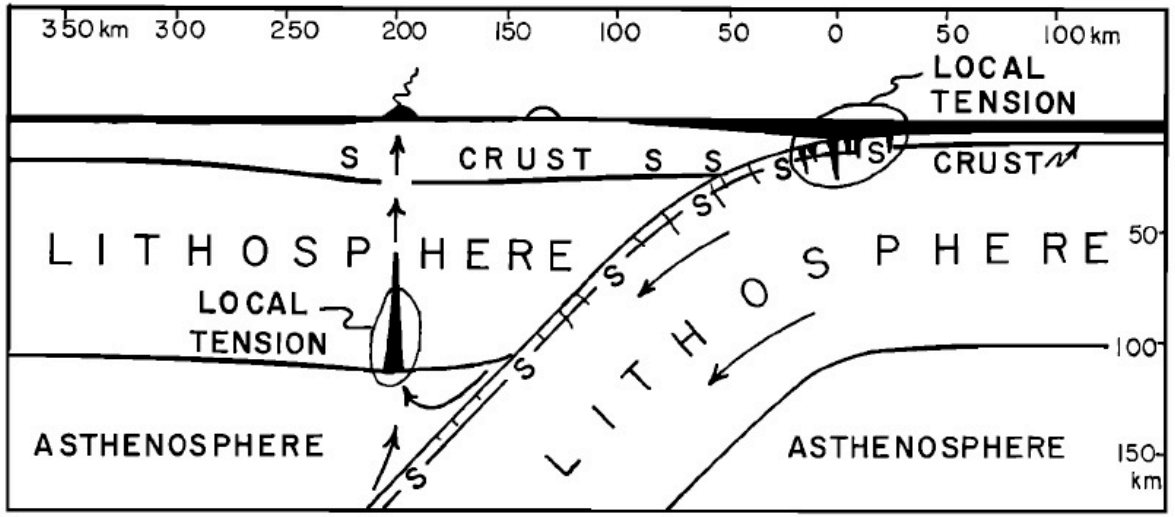

Fig. 7*b*.

Figure 7 shows vertical sections through an island arc indicating hypothetical structures and other features. Both sections show down-going slab of lithosphere, seismic zone near surface of slab and in adjacent crust, tensional features beneath ocean deep where slab bends abruptly and surface is free. (In both sections, *S* indicates seismic activity.) (*a*) A gap in mantle portion of lithosphere beneath island arc and circulation in mantle associated with crustal material of the slab and with adjoining mantle [*Holmes*, 1965]. (*b*) The overriding lithosphere in contact with the down-going slab and bent upward as a result of overthrusting. The relation of the bending to the volcanoes follows *Gunn* [1947]. No vertical exaggeration.

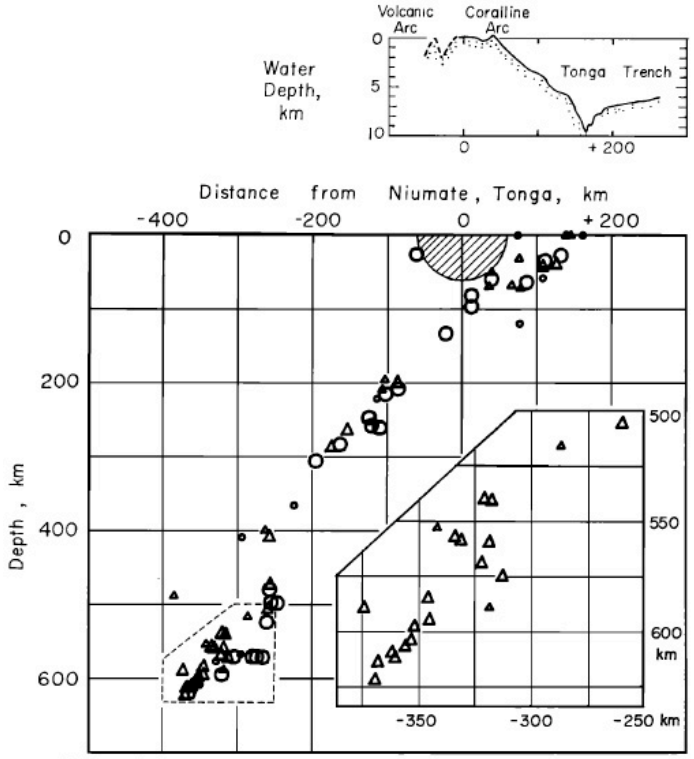

Fig. 9. Vertical section oriented perpendicular to the Tonga arc. Circles represent earthquakes projected from within 0 to 150 km north of the section; triangles correspond to events projected from within 0 to 150 km south of the section. All shocks occurred during 1965 while the Lamont network of stations in Tonga and Fiji was in operation. Locations are based on data from these stations and from more distant stations. No microearthquakes from a sample of 750 events originated from within the hatched region near the station at Niumate, Tonga (i.e., for *S-P* times less than 0.5 sec). A vertical exaggeration of about 13:1 was used for the insert showing the topography [after *Raitt et al.*, 1955]; the horizontal and vertical scales are equal in the cross section depicting earthquake locations. Lower insert shows enlargement of southern half of section for depths between 500 and 625 km. Note small thickness (less than ~20 km) of seismic zone for wide range of depths.

Isacks et al 1968

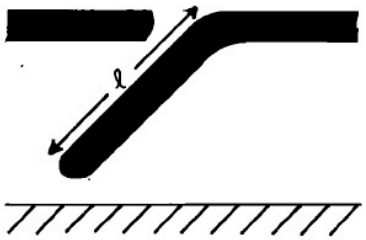

Fig. 14*a*. Length l is a measure of the amount of underthrusting during the most recent period of sea-floor spreading.

Fig. 14*b*. Lithosphere is deformed along its lower edge as it encounters a more resistant layer (the mesosphere).

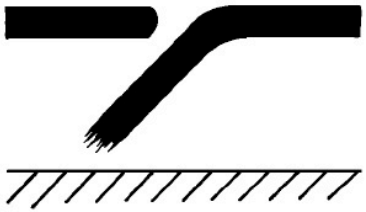

Fig. 14*c*. Length of seismic zone is the product of rate of underthrusting and time constant for assimilation of slab by upper mantle.

Fig. 14*d*. A piece (or pieces) of the lithosphere becomes detached either by gravitational sinking or by forces in the asthenosphere.

Figure 14 shows four possible configurations of an underthrust plate of lithosphere in island arcs. Solid areas indicates lithosphere; white area, asthenosphere; hatched area, mesosphere.

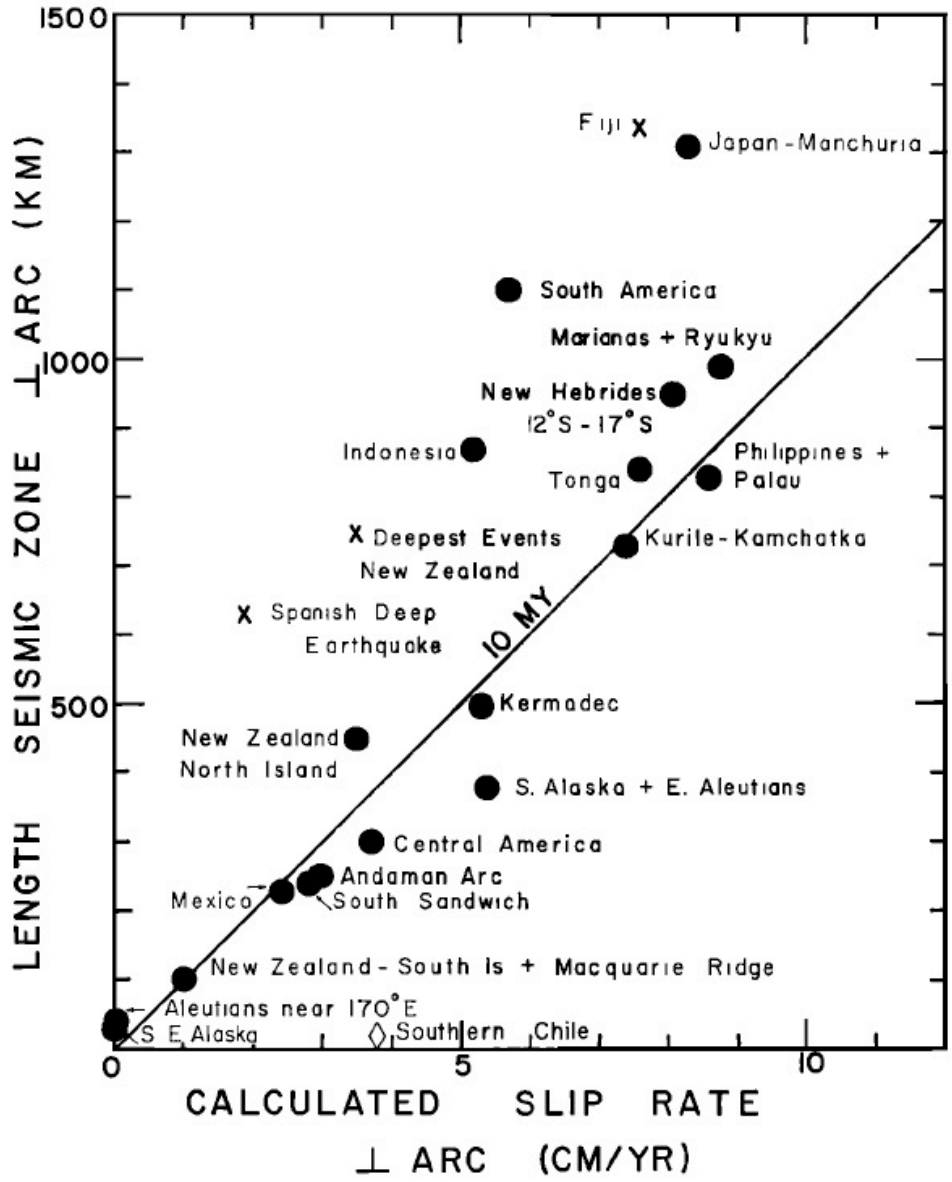

Fig. 16. Calculated rates of underthrusting [*Le Pichon*, 1968], and length of seismic zone for various island arcs and arc-like features (solid circles), for several unusual deep events (crosses), and for Southern Chile (diamond). The solid line indicates the theoretical locus of points for uniform spreading over a 10-m.y. interval.

Isacks et al 1968

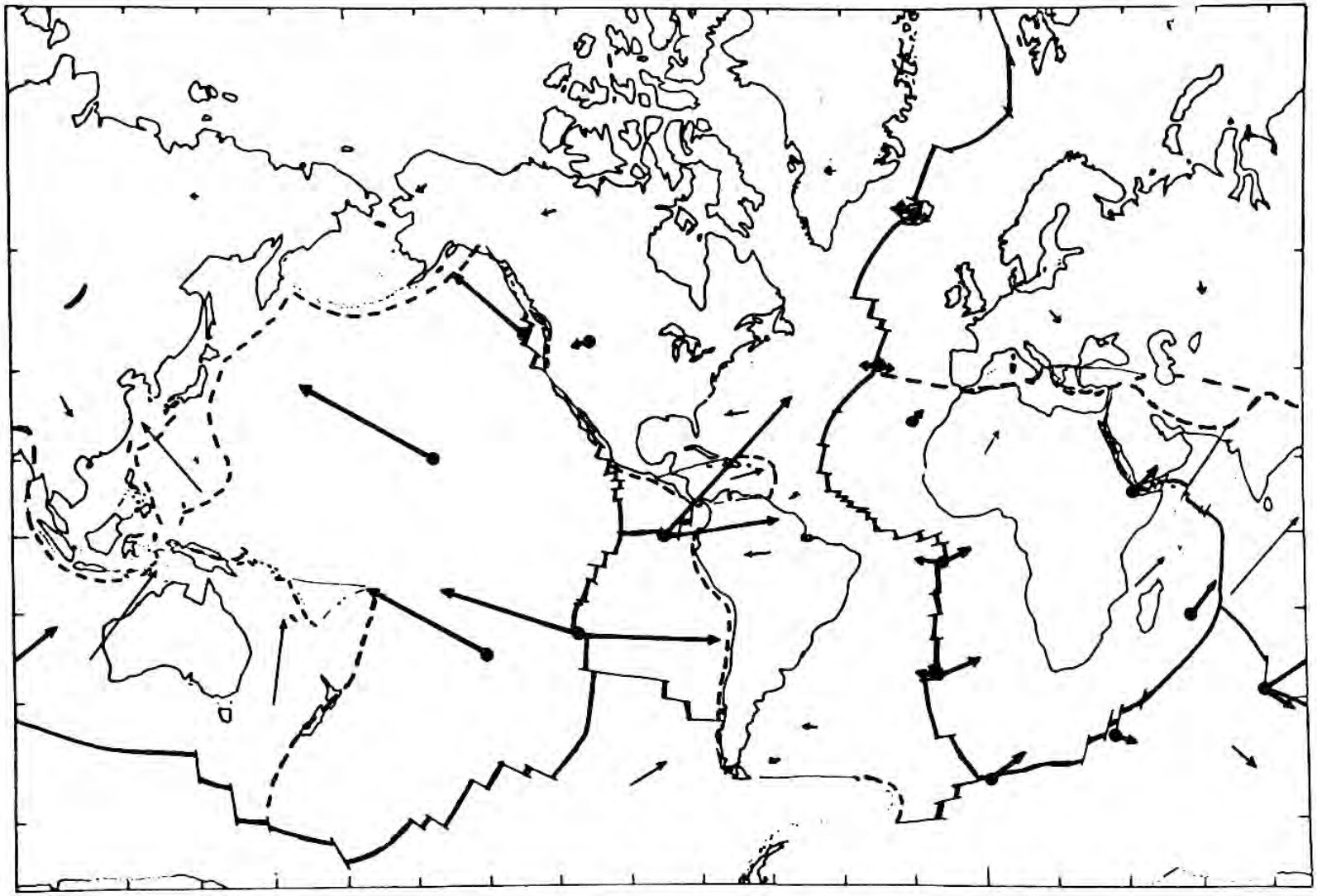

Figure 49-1
The arrows show the direction and speed of the plates over the mantle: the heavier arrows show the plate motion at hotspots. This synthesis was based on relative plate motion data (fault strikes and spreading rates) and predicts the directions of the aseismic ridges/island chains emanating from the hotspots

Morgan 1971

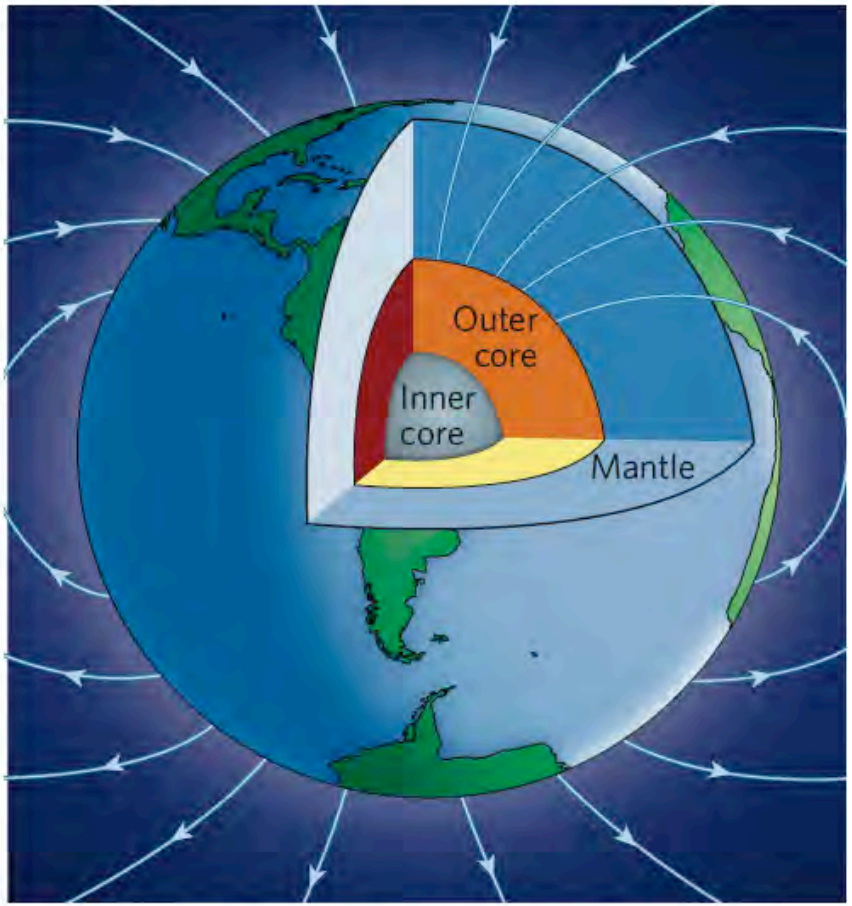

Figure 1 | Earth's magnetic field. The field looks like that of a bar magnet aligned with Earth's geographical axis, a so-called dipole structure. The non-dipole part of the field is significant, however, and accounts for why the compass rarely points exactly to true north. The field is generated in Earth's liquid outer core, some 3,000 kilometres below us; the rocky solid mantle is a fairly good electrical insulator and most of it is too hot to be magnetized, so it does not affect the field much.

Gubbins 2008

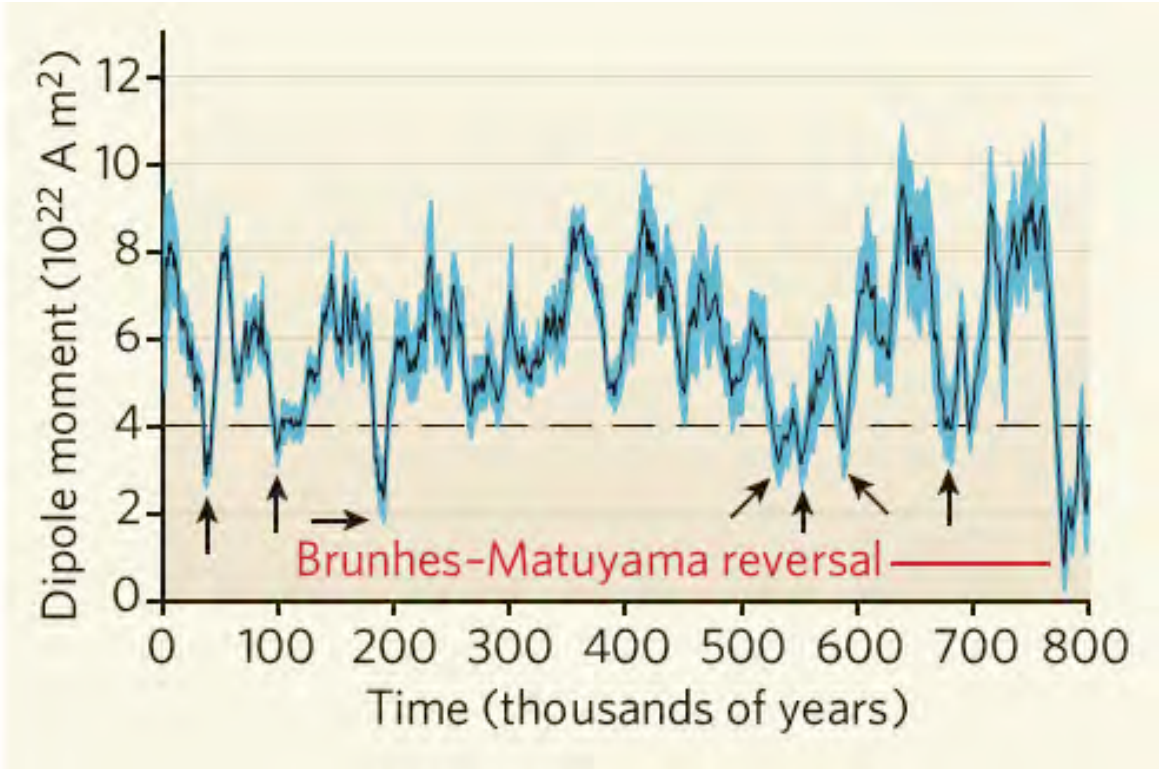

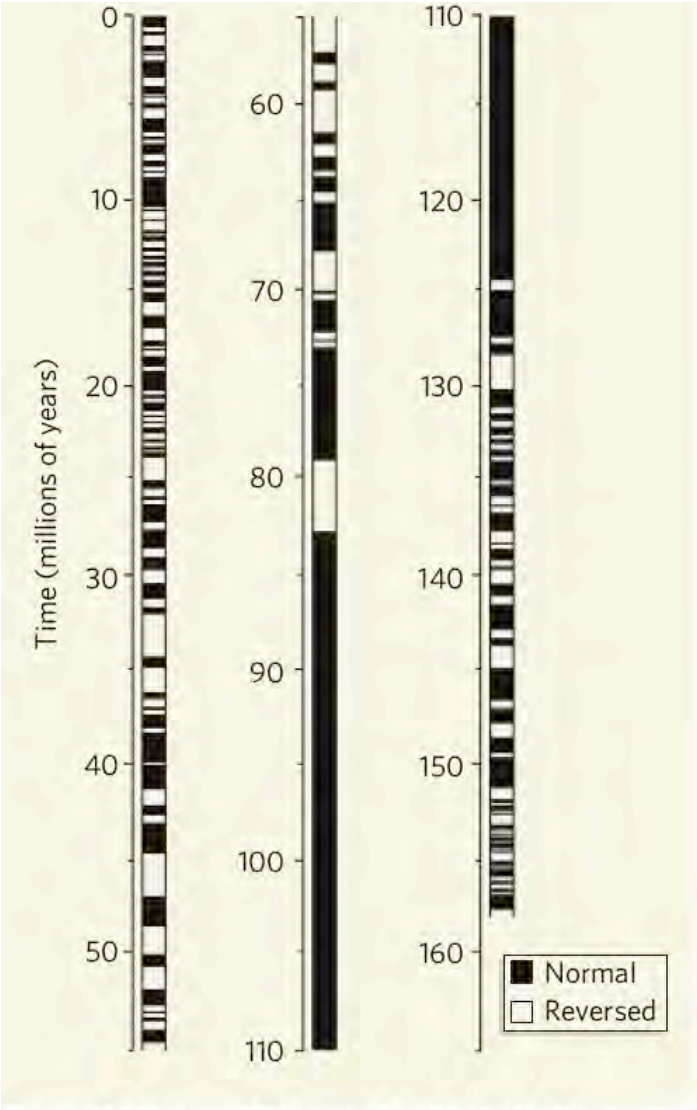

Figure 4 | Reversal timescale. Note the long black interval when the polarity was normal and there were no reversals, the so-called Cretaceous normal superchron (CNS). It may also be possible to discern an increase in the frequency of reversals since 80 million years ago, when the CNS ceased. (Revised from W. Lowrie

Gubbins 2008

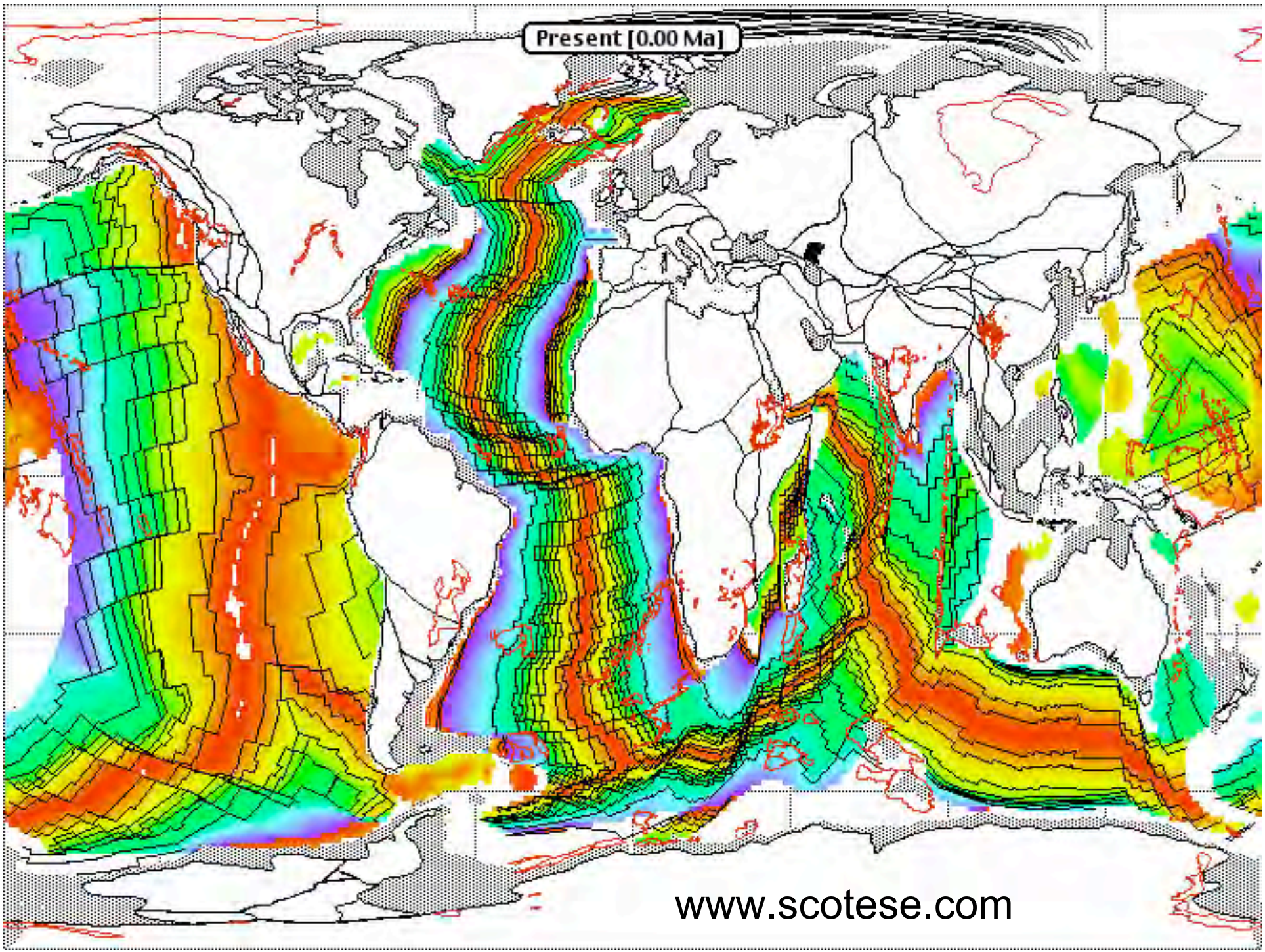
Present [0.00 Ma]
www.scotese.com

Eyjafjallajfull Eruption: March 27, 2010

http://www.flickr.com/photos/orvaratli/4476862865/

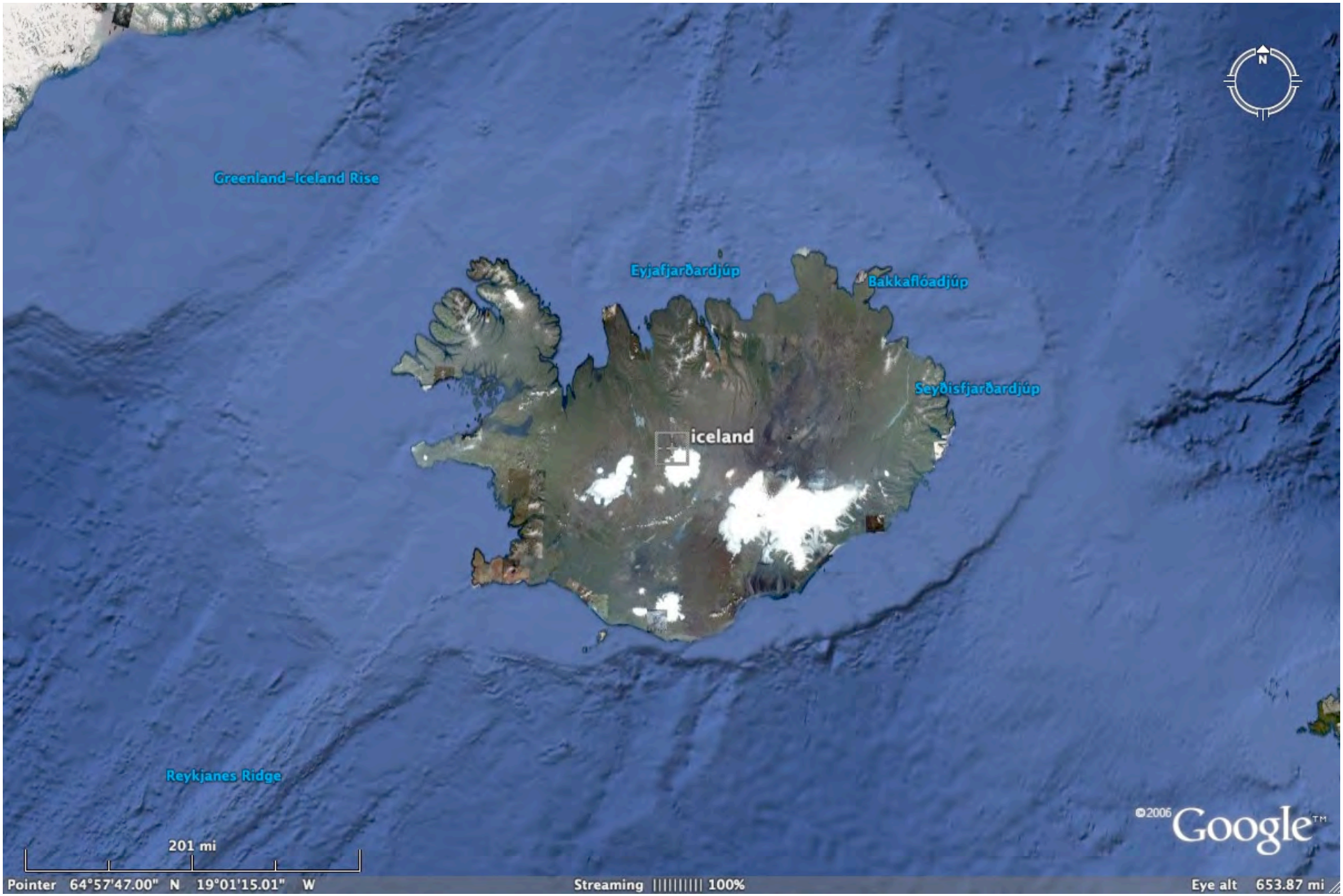
Greenland-Iceland Rise
Eyjafjarðardjúp
Bakkaflóadjúp
Seyðisfjarðardjúp
iceland
Reykjanes Ridge
201 mi
©2006 Google™
Pointer 64°57'47.00" N 19°01'15.01" W
Streaming 100%
Eye alt 653.87 mi


N
© 2010 Europa Technologies
© 2010 Google
©2006 Google™
7.04 mi
Pointer 66°24'05.11" N 16°10'32.55" W
Streaming 100%
Eye alt 24.28 mi


N
© 2010 Europa Technologies
© 2010 Google
©2006 Google™
18.3 mi
Pointer 65°24'31.28" N 17°03'31.45" W
Streaming 100%
Eye alt 62.86 mi

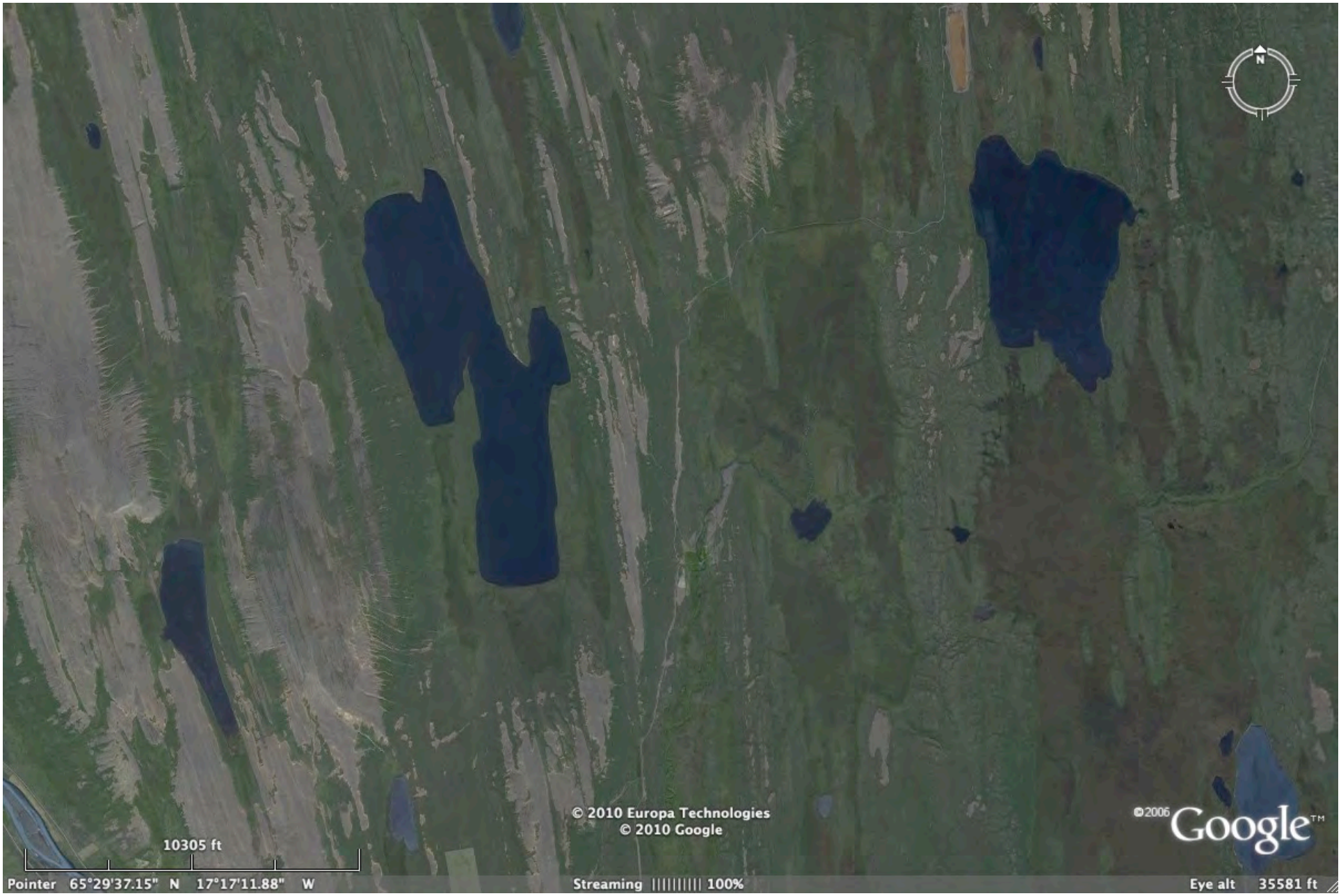
N
© 2010 Europa Technologies
© 2010 Google
©2006 Google™
10305 ft
Pointer 65°29'37.15" N 17°17'11.88" W
Streaming 100%
Eye alt 35581 ft

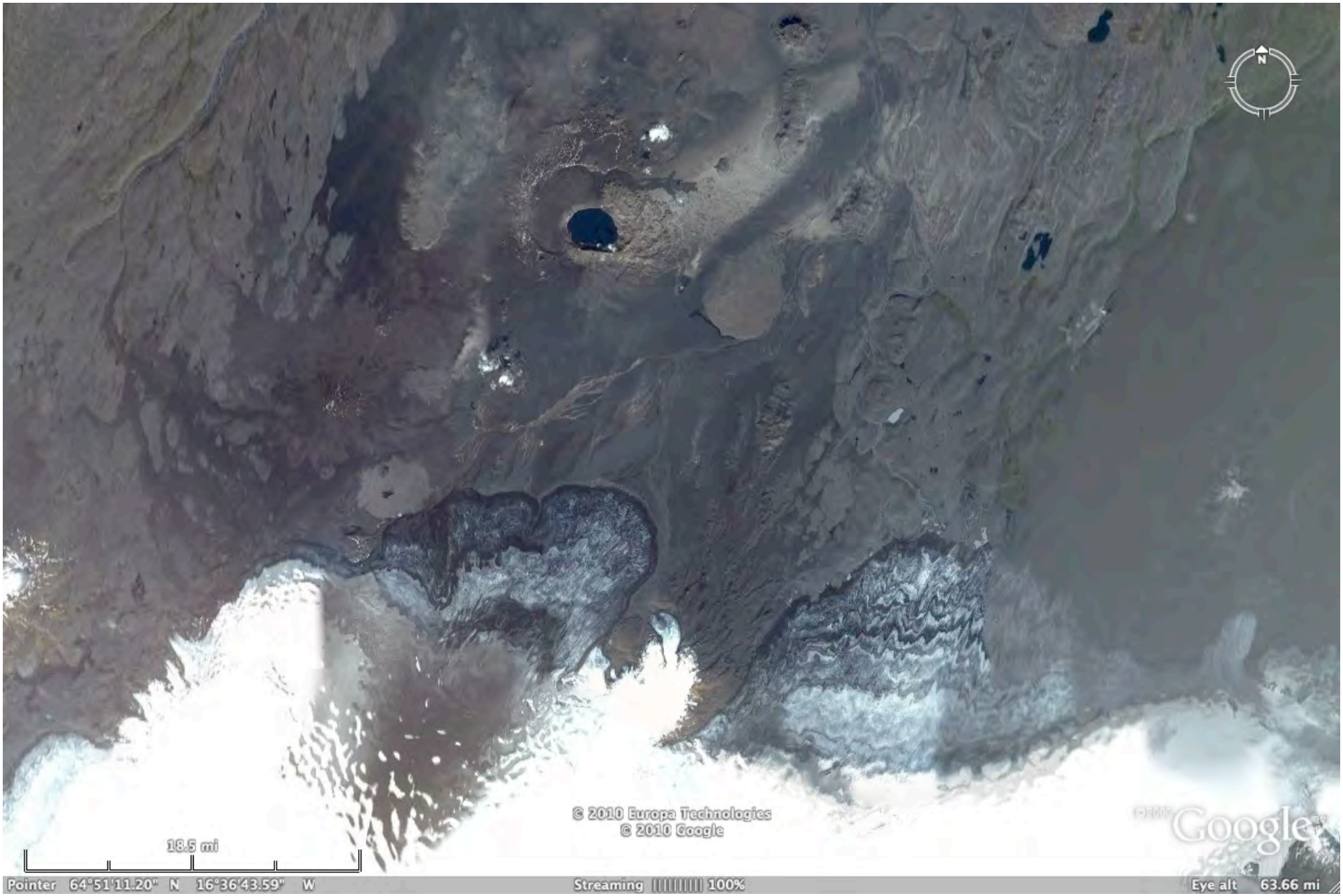
N
© 2010 Europa Technologies
© 2010 Google
Google
18.5 mi
Pointer 64°51'11.20" N 16°36'43.59" W
Streaming 100%
Eye alt 63.66 mi


N
© 2010 Europa Technologies
© 2010 Google
©2006 Google™
2.11 mi
Pointer 65°01'28.57" N 16°43'28.96" W
Streaming 100%
Eye alt 38461 ft

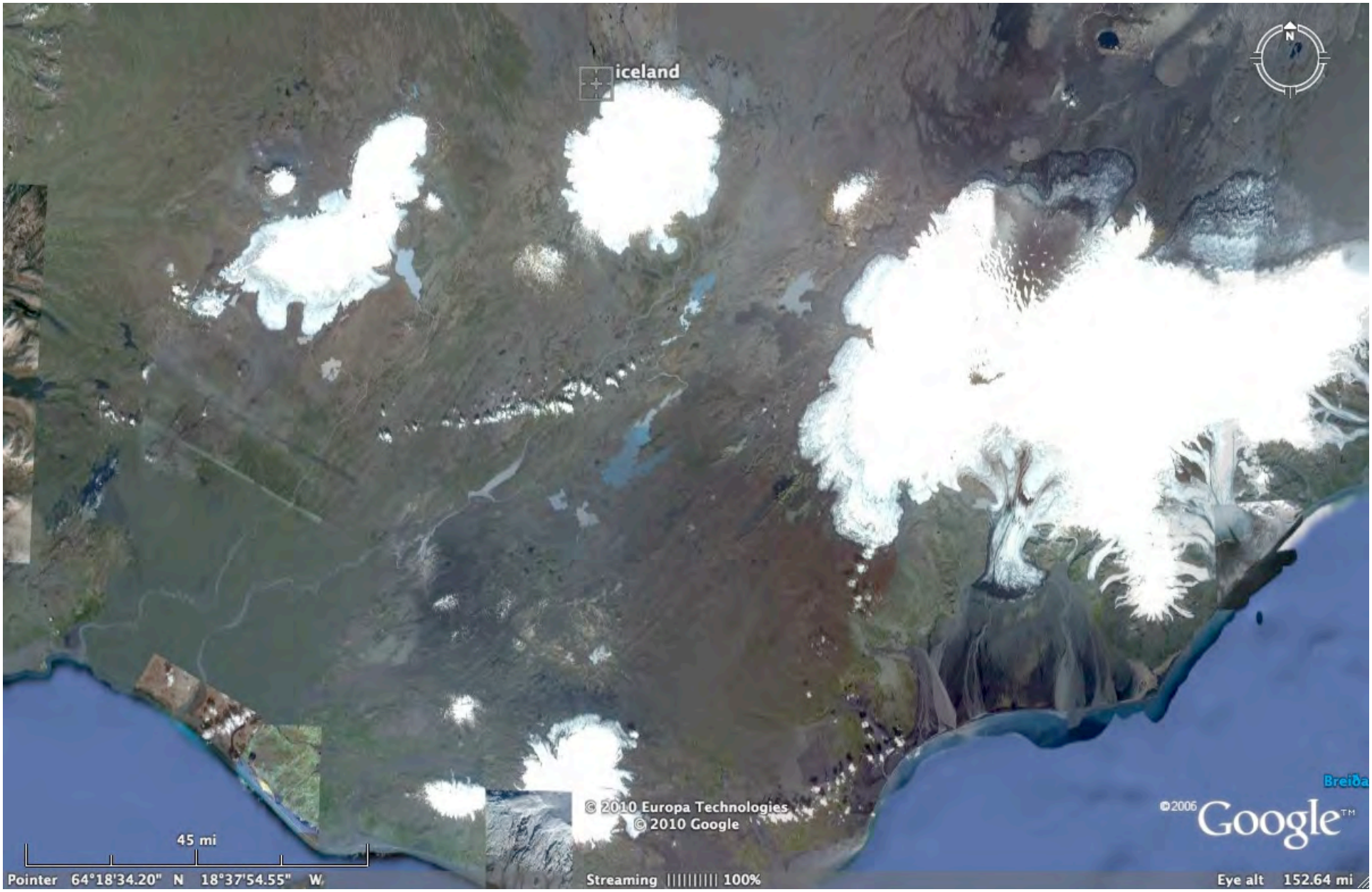
iceland
N
© 2010 Europa Technologies
© 2010 Google
©2006 Google™
45 mi
Pointer 64°18'34.20" N 18°37'54.55" W
Streaming 100%
Eye alt 152.64 mi

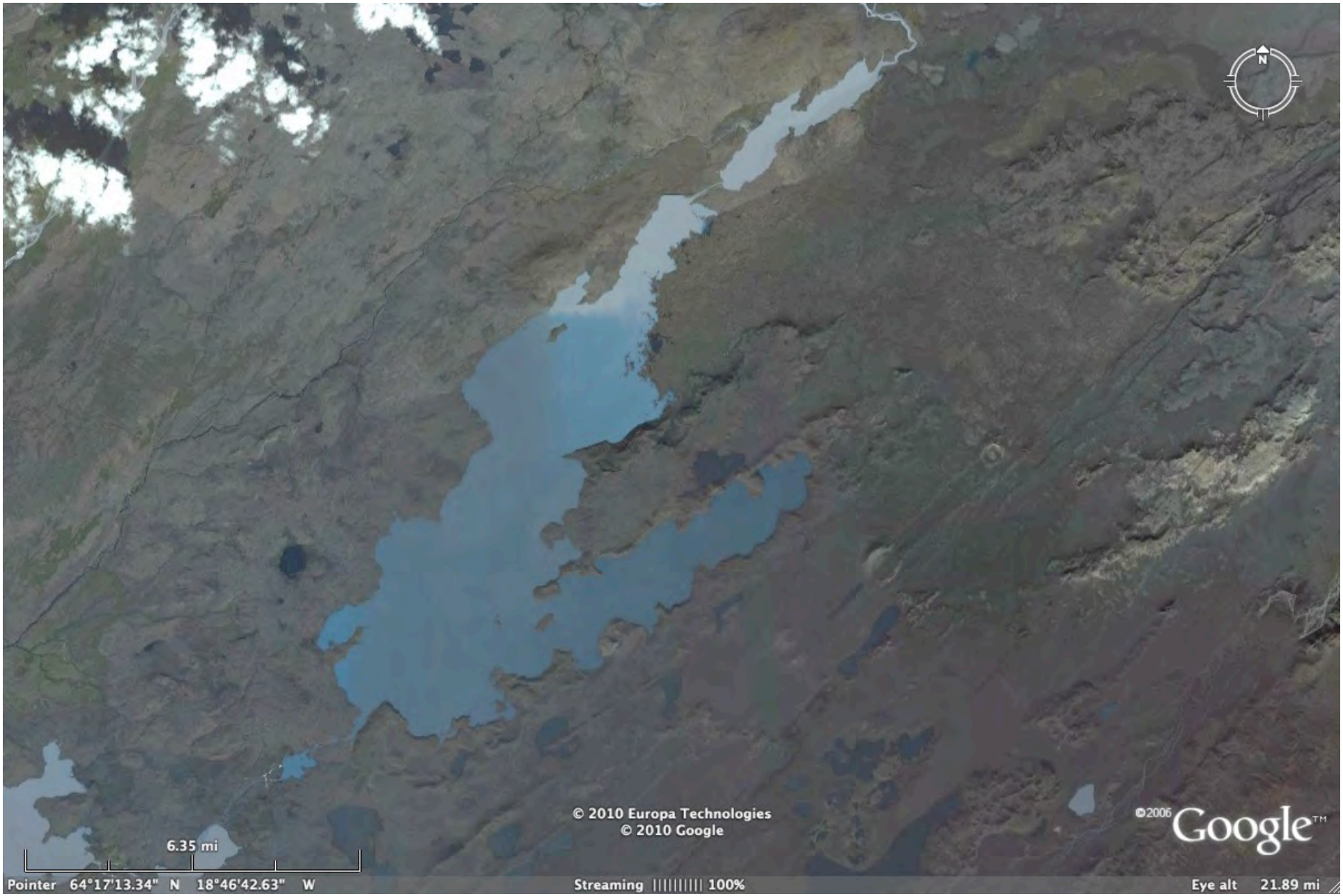
N
© 2010 Europa Technologies
© 2010 Google
©2006 Google™
6.35 mi
Pointer 64°17'13.34" N 18°46'42.63" W
Streaming 100%
Eye alt 21.89 mi


Jökuldjúp
iceland
N
© 2010 Europa Technologies
© 2010 Google
©2006 Google™
78 mi
Pointer 63°51'11.39" N 22°36'09.21" W
Streaming 100%
Eye alt 262.76 mi

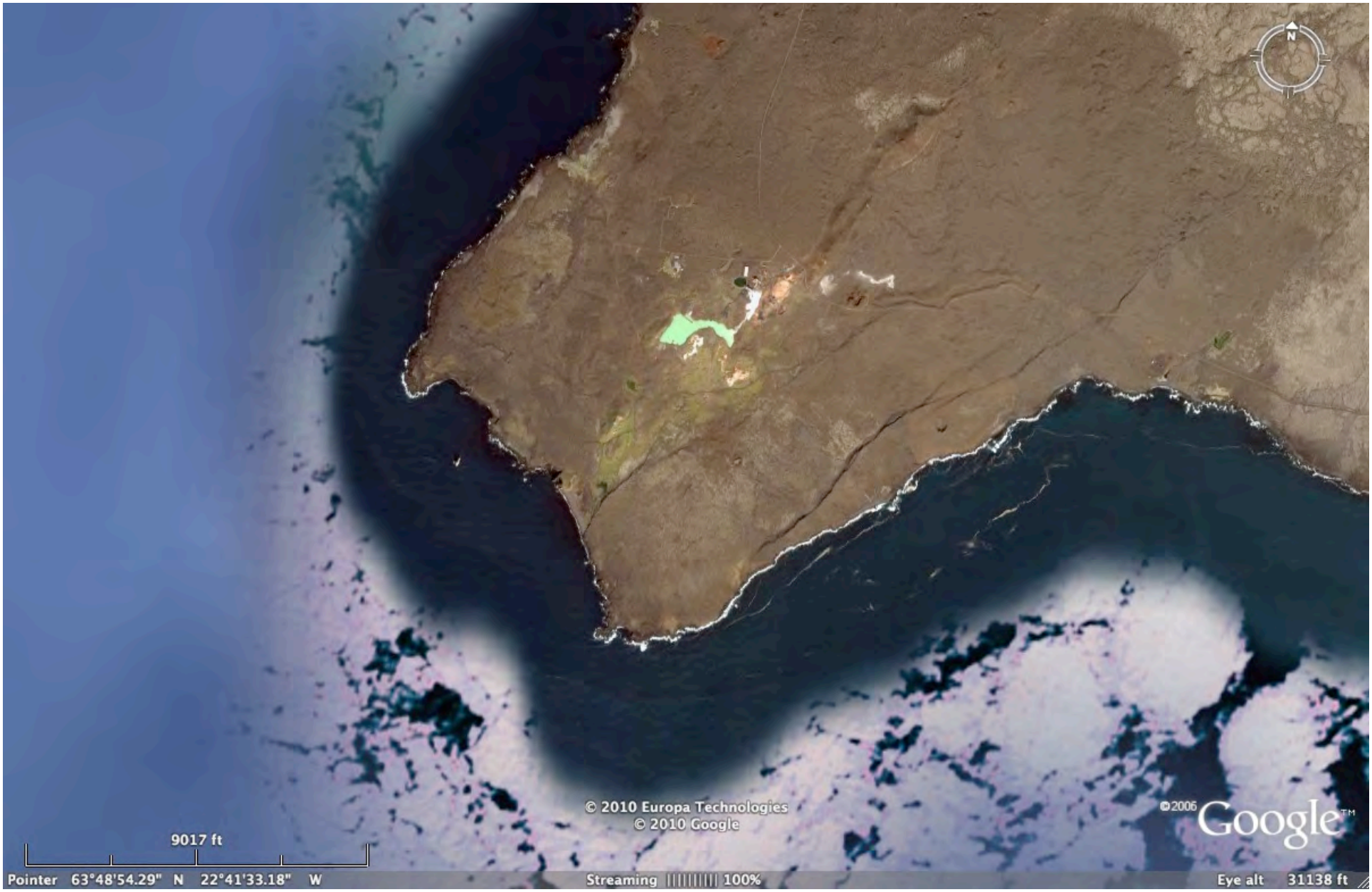
N
© 2010 Europa Technologies
© 2010 Google
©2006 Google™
9017 ft
Pointer 63°48'54.29" N 22°41'33.18" W
Streaming 100%
Eye alt 31138 ft


N
© 2010 Europa Technologies
© 2010 Google
©2006 Google™
3589 ft
Pointer 63°48'58.67" N 22°42'27.57" W
Streaming 100%
Eye alt 12397 ft


Tjornes Peninsula: Miocene marine strata
http://www.flickr.com/photos/s_r_in_iceland/1322711591/sizes/o/

Brekkufjall: Miocene Plateau Basalts

http://www.flickr.com/photos/iceland-ho/3792564256/sizes/l/in/photostream/

Holocene dike
Intruding
Holocene tephra
Reykjanesta

http://www.flickr.com/photos/hmh/304518586/

Almannagja: normal fault & rift valley

http://www.flickr.com/photos/mundilfari_gjk/2324579720/

Oraefajokull: Composit Volcano & Ice Cap

http://www.flickr.com/photos/21527076@N08/2155336887/

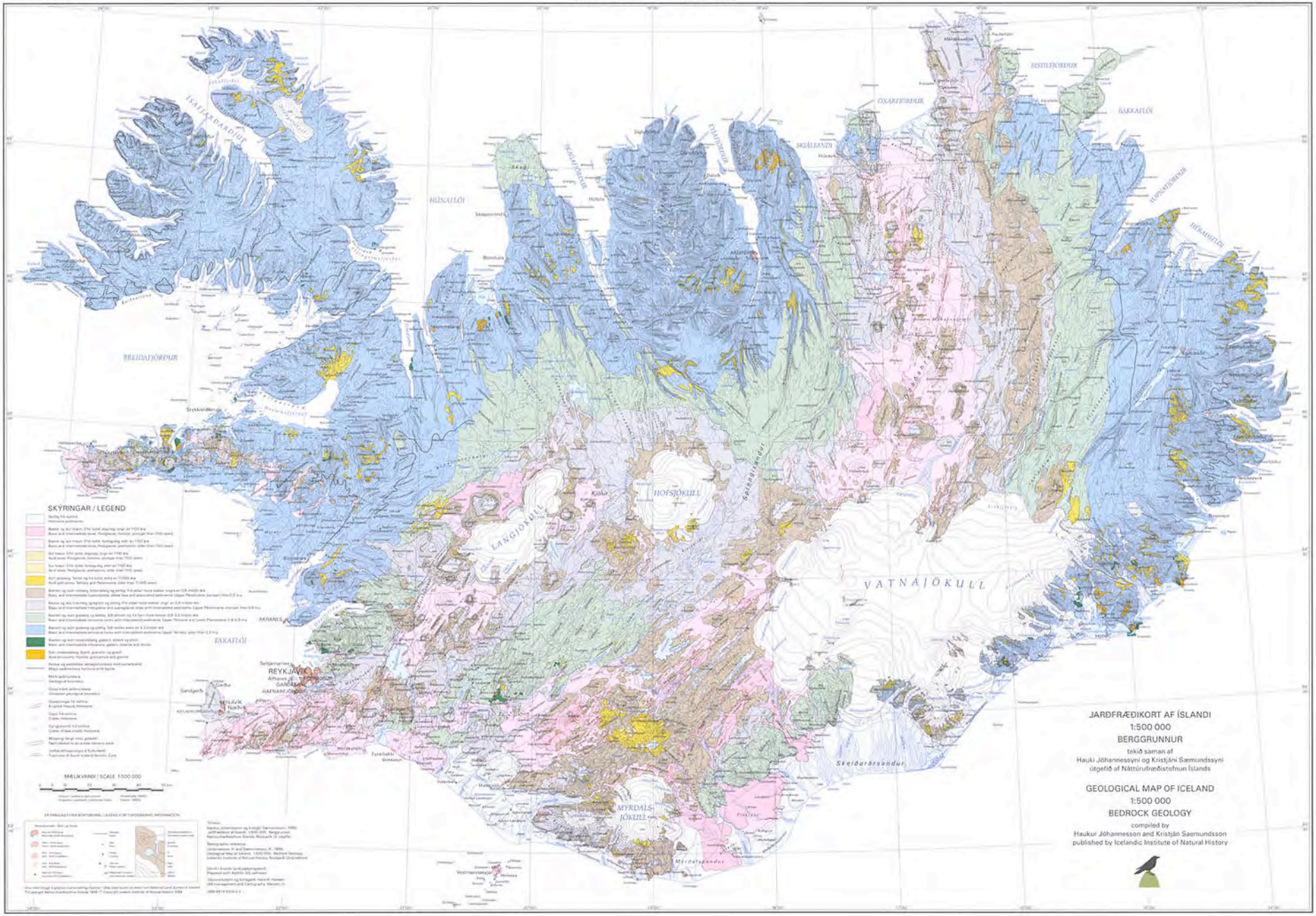
SKÝRINGAR / LEGEND
MÆLIKVARÐI / SCALE 1:500 000
JARÐFRÆÐIKORT AF ÍSLANDI
1:500 000
BERGGRUNNUR
tekið saman af
Hauki Jóhannessyni og Kristjáni Sæmundssyni
útgefið af Náttúrufræðistofnun Íslands
GEOLOGICAL MAP OF ICELAND
1:500 000
BEDROCK GEOLOGY
compiled by
Haukur Jóhannesson and Kristján Sæmundsson
published by Icelandic Institute of Natural History
REYKJAVÍK
HOFSJÖKULL
LANGJÖKULL
VATNAJÖKULL
MÝRDALS JÖKULL
ÍSAFJARÐARDJÚP
HÚNAFLÓI
BREIÐAFJÖRÐUR
FAXAFLÓI
ÖXARFJÖRÐUR
SKJÁLFANDI
BAKKAFLÓI
Skeiðarársandur
Mýrdalssandur

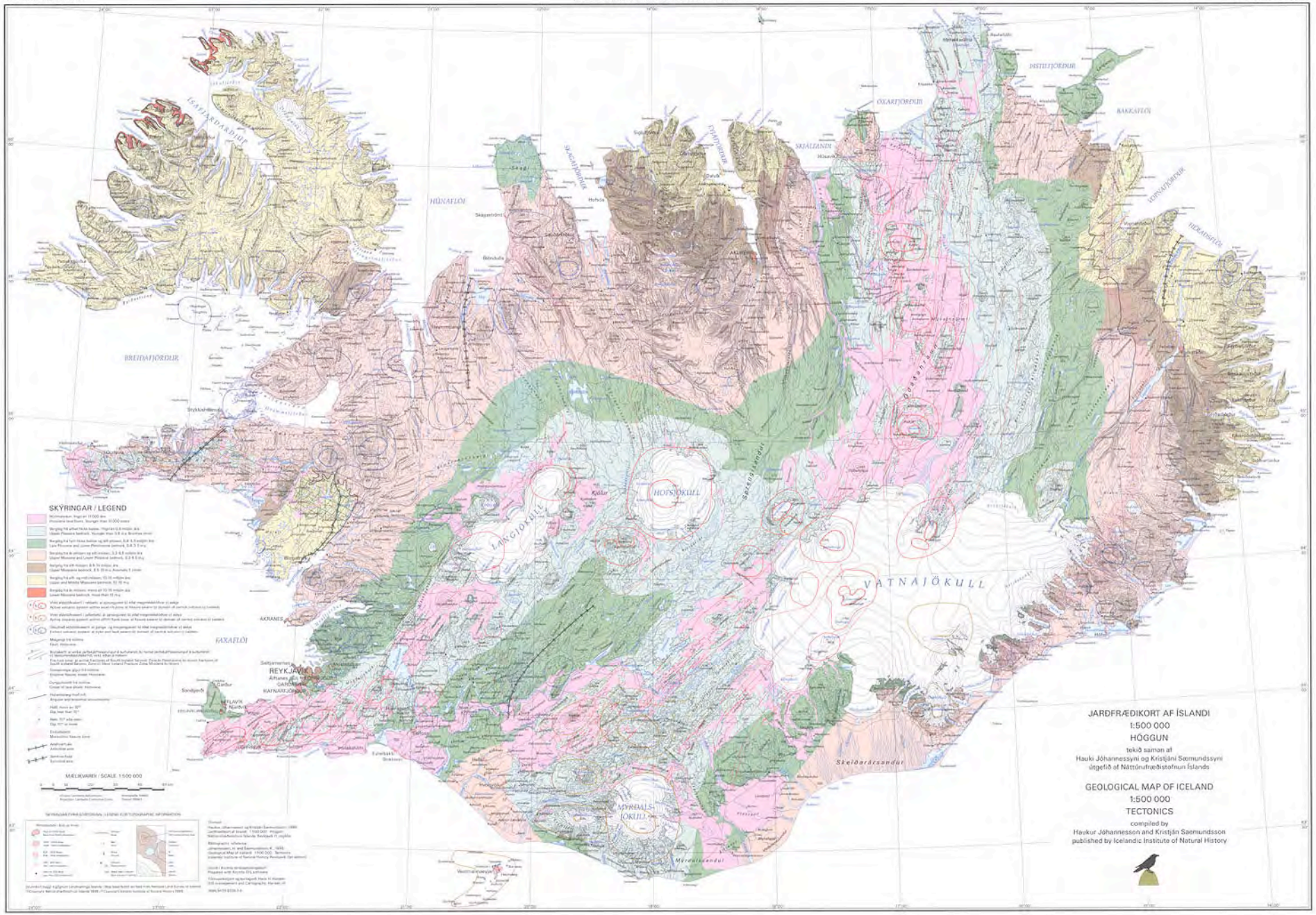
SKÝRINGAR / LEGEND
MÆLIKVARÐI / SCALE 1:500 000
JARÐFRÆÐIKORT AF ÍSLANDI
1:500 000
HÖGGUN
tekið saman af
Hauki Jóhannessyni og Kristjáni Sæmundssyni
útgefið af Náttúrufræðistofnun Íslands
GEOLOGICAL MAP OF ICELAND
1:500 000
TECTONICS
compiled by
Haukur Jóhannesson and Kristján Sæmundsson
published by Icelandic Institute of Natural History
BREIÐAFJÖRÐUR
HÚNAFLÓI
SKAGAFJÖRÐUR
EYJAFJÖRÐUR
SKJÁLFANDI
ÖXARFJÖRÐUR
ÞISTILFJÖRÐUR
BAKKAFLÓI
VOPNAFJÖRÐUR
HÉRAÐSFLÓI
FAXAFLÓI
REYKJAVÍK
HOFSJÖKULL
LANGJÖKULL
VATNAJÖKULL
MÝRDALSJÖKULL
Skeiðarársandur
Mýrdalssandur

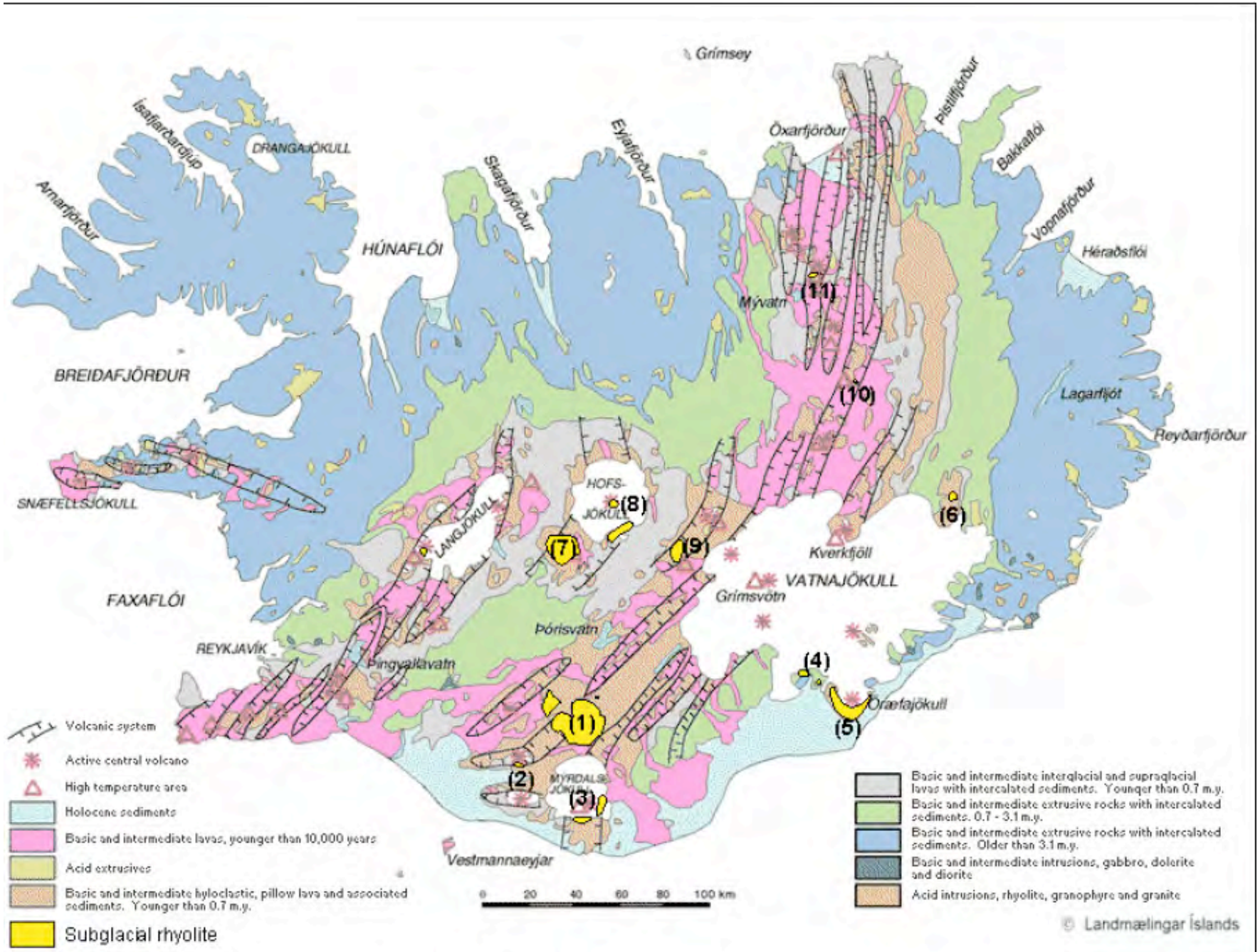

(1) Torfajökul. (2) Tindfjallajökull. (3) Mýrdalsjökull. (4) Skaftafellsfjöll. (5) Oræfajökull. (6) Snæfell. (7) Kerlingarfjöll. (8) Ármafell and Hásteinar. (9) Hágöngur. (10) Eggert. (11) Hliðarfjall.

Norodahl et al 2008

Ca 13000 ^{14}C BP

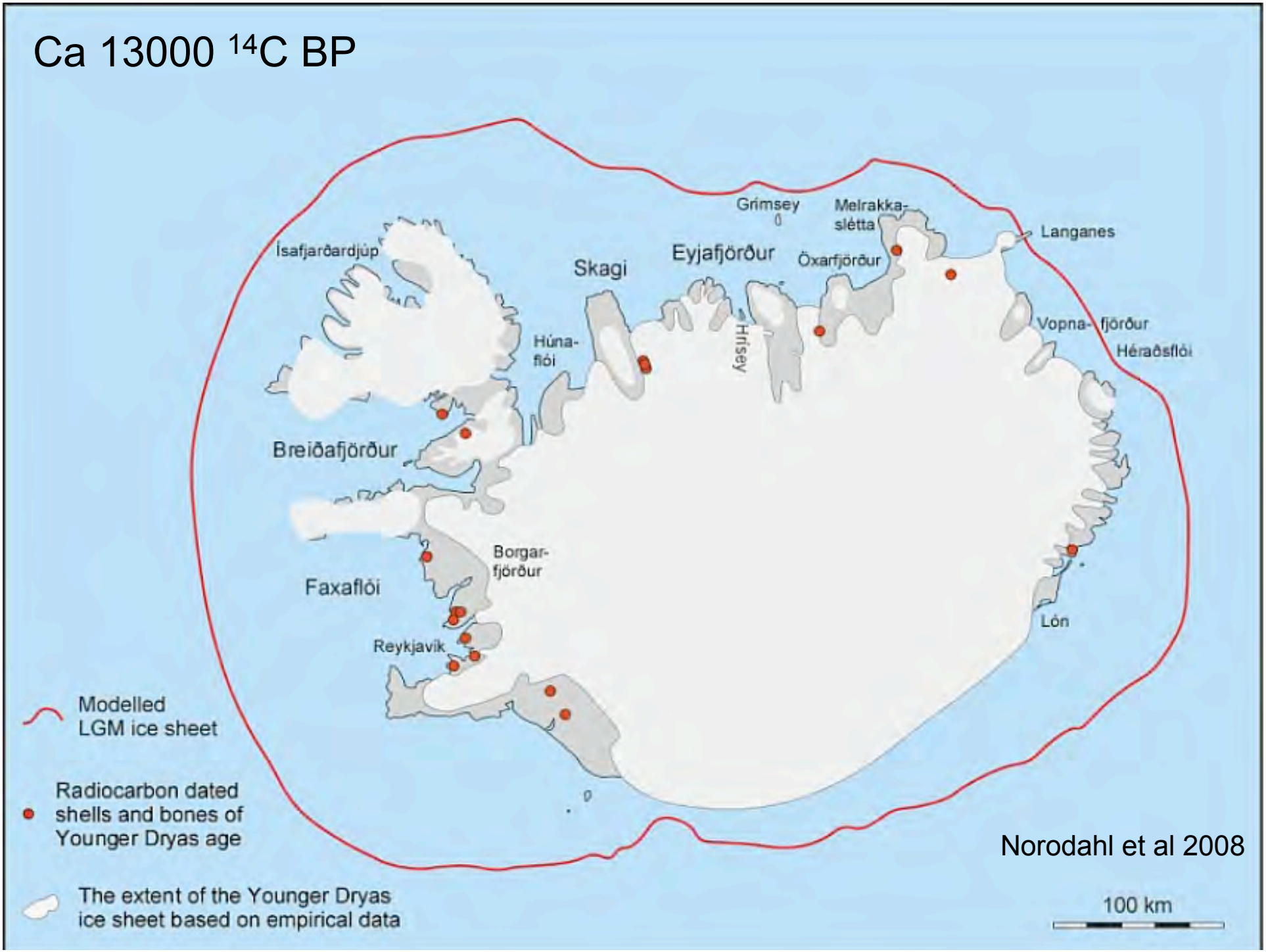

Norodahl et al 2008

Ca 9,800 ^{14}C BP

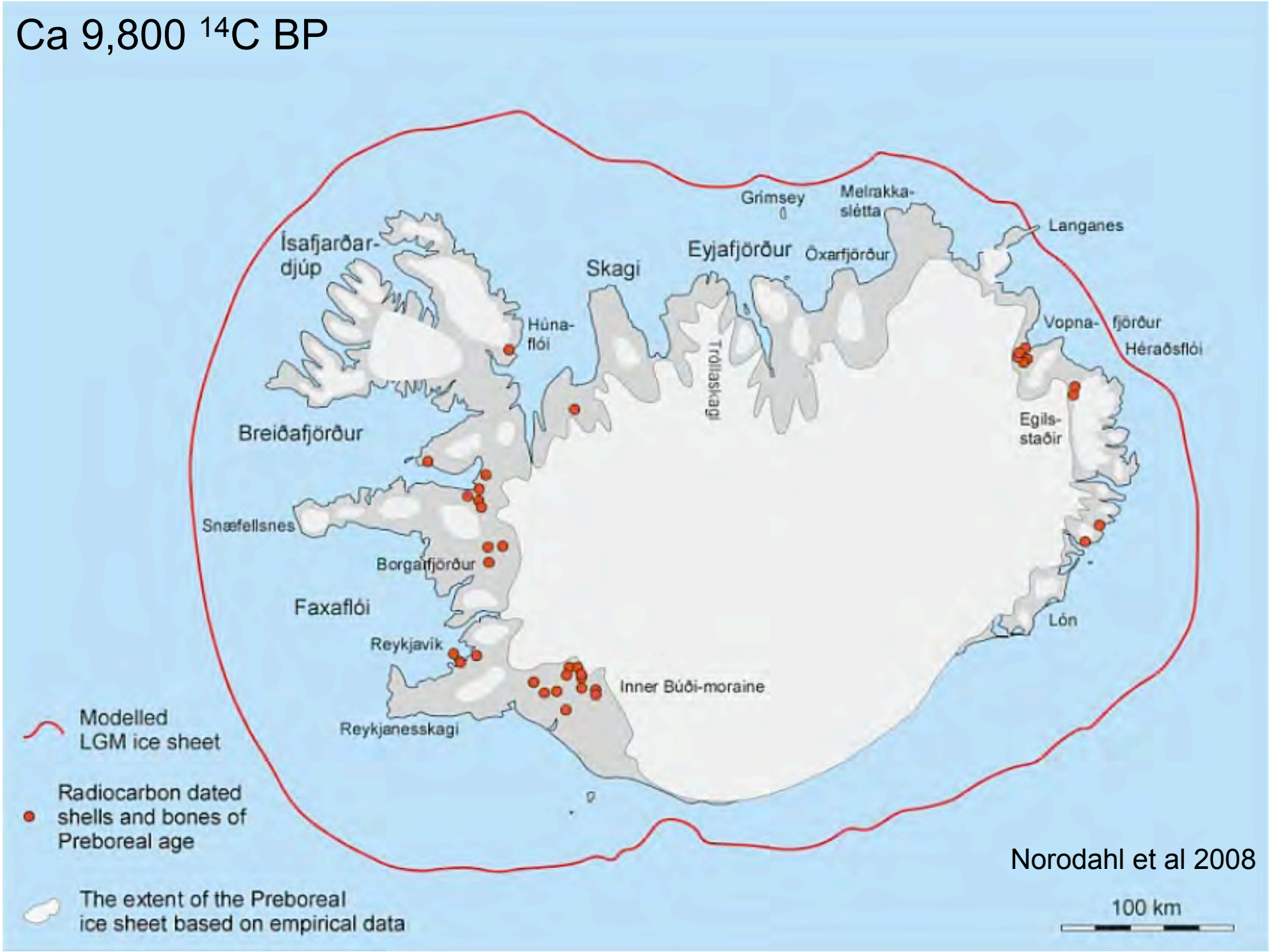

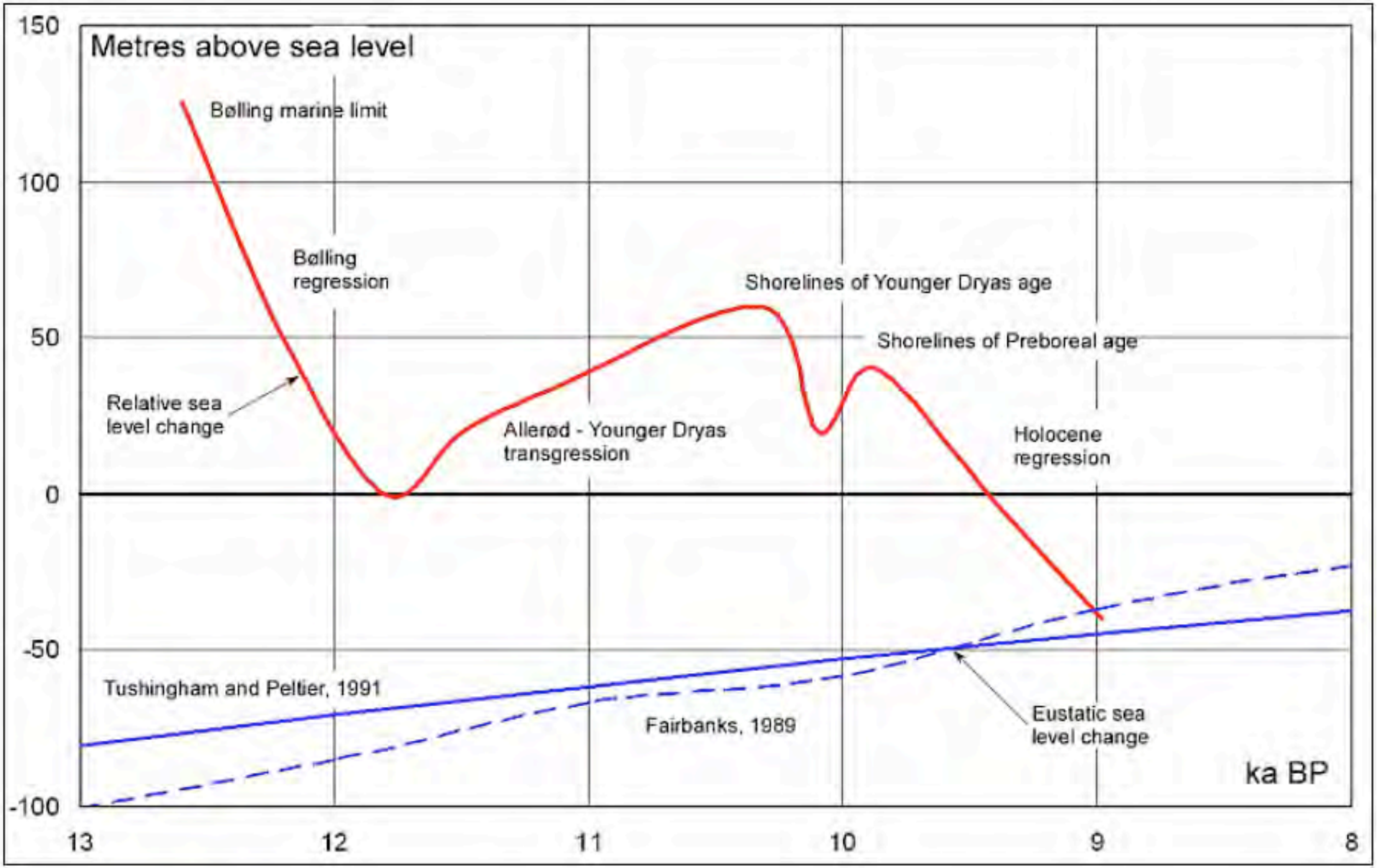

Norodahl et al 2008

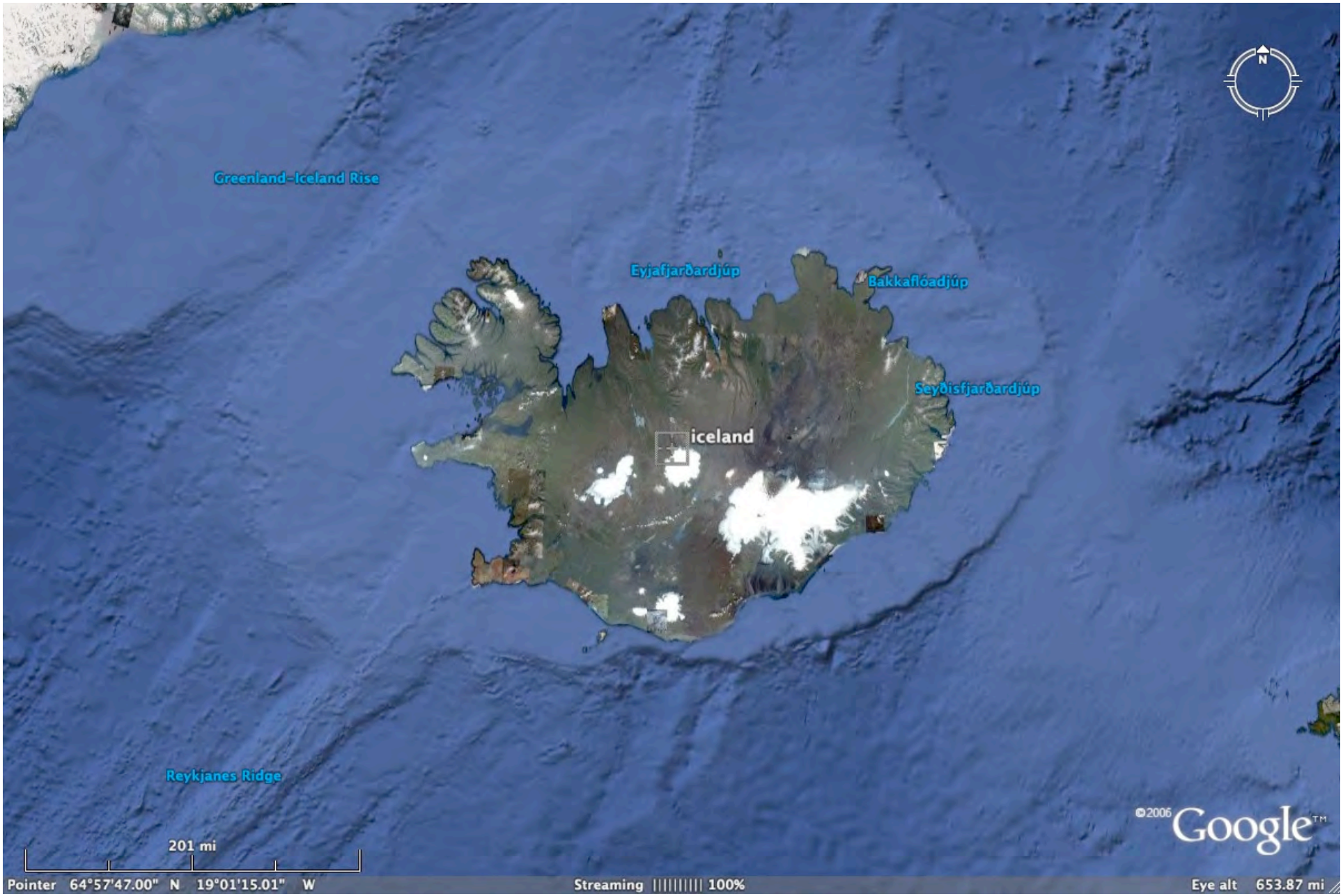
Greenland-Iceland Rise
Eyjafjarðardjúp
Bakkaflóadjúp
Seyðisfjarðardjúp
iceland
Reykjanes Ridge
201 mi
©2006 Google™
Pointer 64°57'47.00" N 19°01'15.01" W
Streaming 100%
Eye alt 653.87 mi

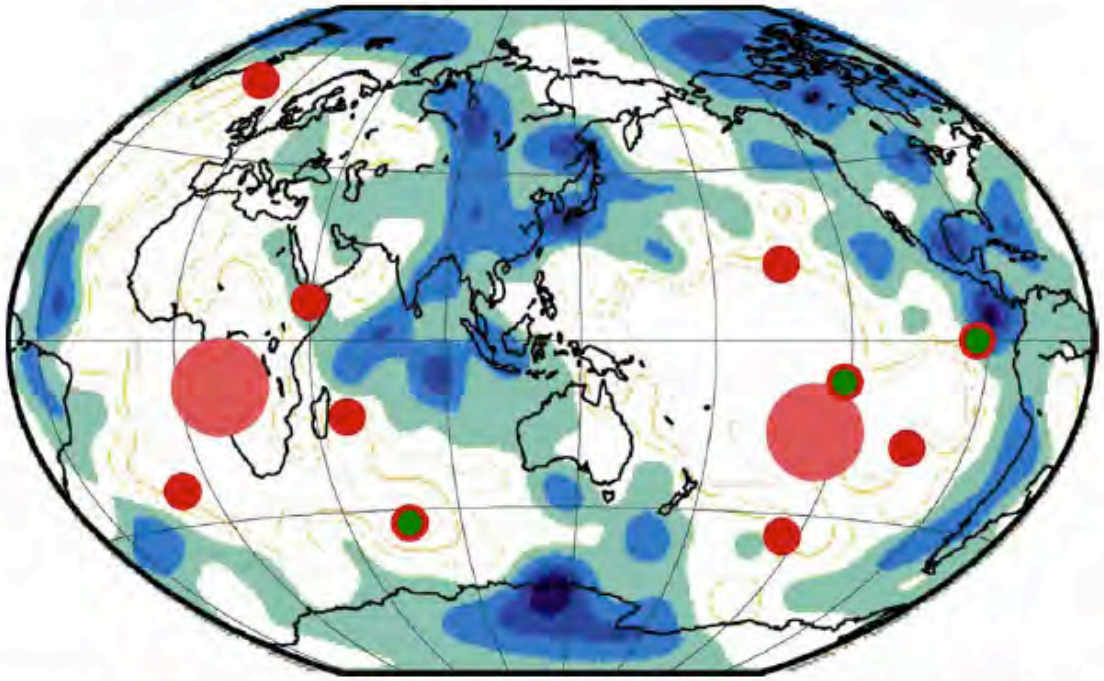

Fig. 3. Primary plumes and superswells shown on a tomographic map of shear wave velocity at 2850 km depth [25]. Only the positive (fast, cold) anomalies are shown in blue shades. The negative (slow, hot) anomalies are in white (the complete tomographic picture is seen in Fig. 1b). The locations of the Pacific and African superswells are indicated as large pink dots. The seven primary hotspots identified in the paper are shown as smaller red dots. Three hotspots that could be part of the primary group (see text) are shown as green dots with red edges. The primary hotspots tend to form above hot regions but away from both superswells and the cold (subduction-related?) belts.

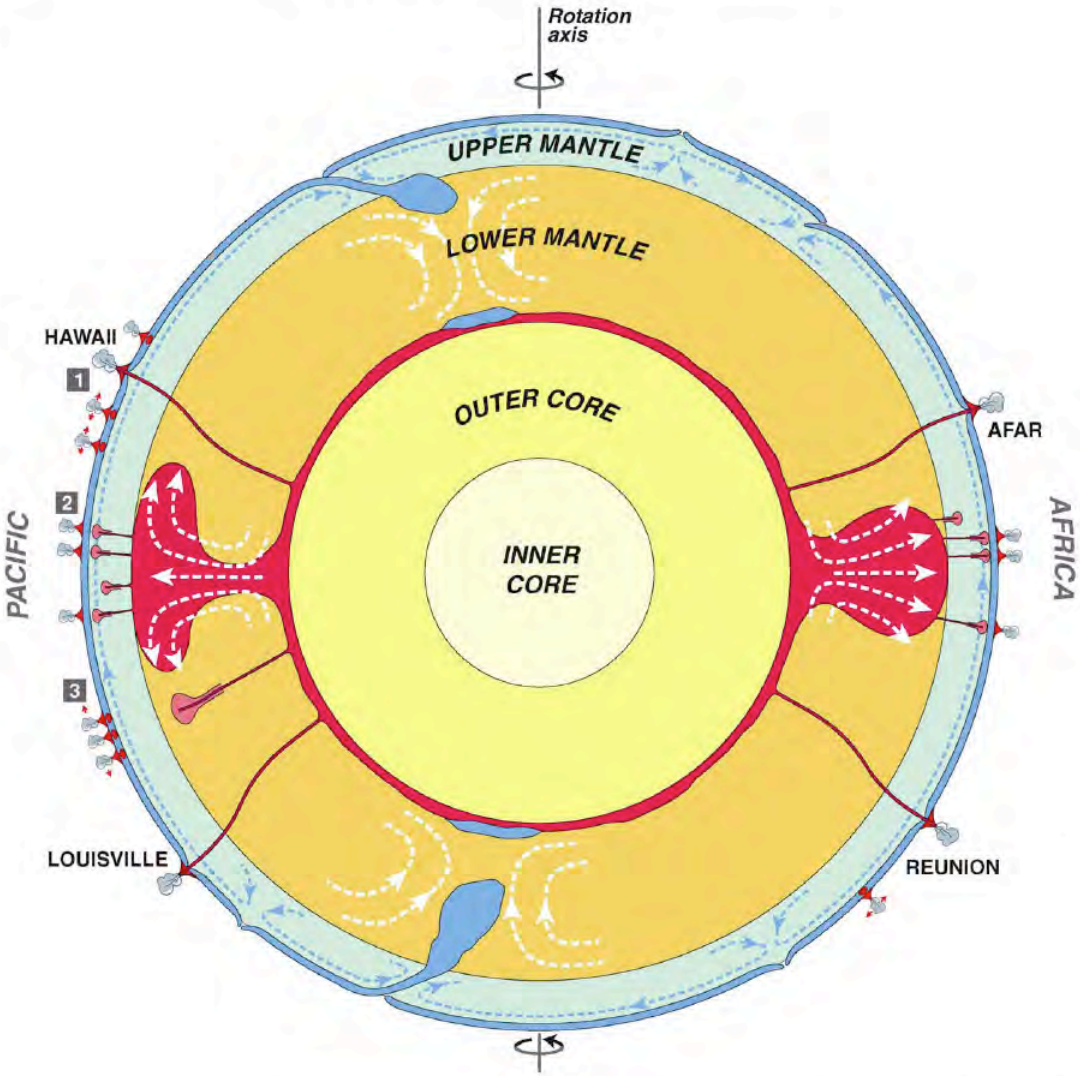

Fig. 4. A schematic cross-section of the dynamic Earth going through its rotation axis, outlining the sources of the three types of plumes/hotspots identified in this paper: the 'primary' or main, deeper plumes possibly coming from the lowermost mantle boundary layer (D″ in the broad sense) are the main topic of the paper; the 'secondary' plumes possibly coming from the top of domes near the depth of the transition zone at the locations of the superswells are indicated [46,47]; the 'tertiary' hotspots may have a superficial origin, linked to tensile stresses in the lithosphere and decompression melting [9,10]. There are on the order of 10 primary (deeper) plumes forming a girdle around the two antipodal domes upwelling below the central Pacific and Africa. At present only plume tails and no plume heads are active and close to the surface, and the number of plumes in a single cross-section is less. The fluid mechanics aspects are based on the experimental study of thermochemical plumes by Davaille et al. [57,58], and the lower mantle domes are based on seismic tomography [25,26]. The location of possible avalanches [63] at the downwellings of the lower mantle quadrupolar convection cells are indicated by sagging in the transition zone, though no such event is thought to be presently active.

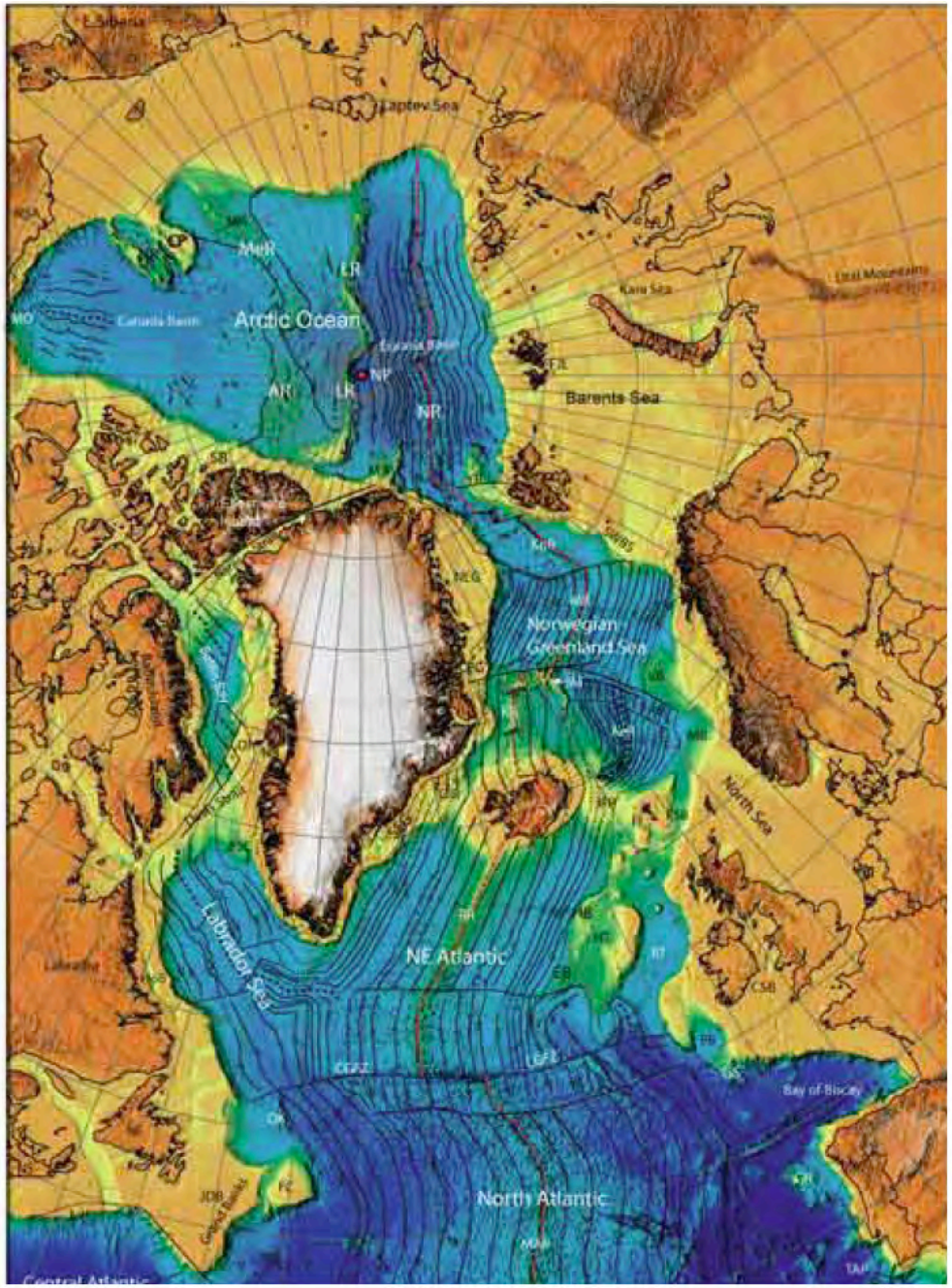

Lundin & Dore
http://www.mantleplumes.org/Iceland2.html

Lundin & Dore
http://www.mantleplumes.org/Iceland2.html

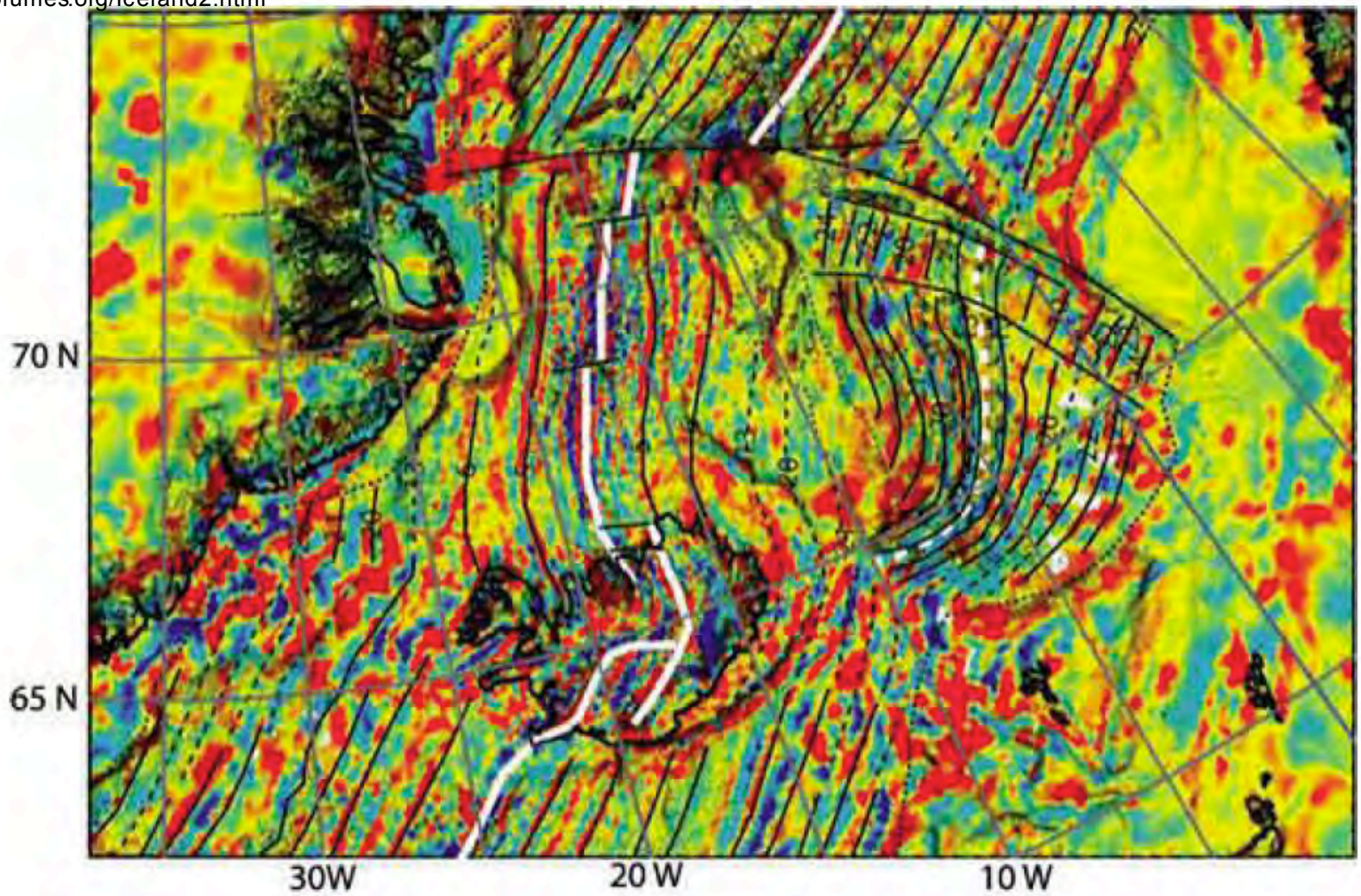

Figure 2a. Shaded relief image of magnetic data (Verhoef et al., 1996) draped on bathymetry (Smith & Sandwell, 1997). Solid white lines = active spreading axes, dashed white line = abandoned Aegir Ridge, thin solid black lines = interpreted magnetic anomalies, thick solid black lines = fracture zones; dotted black lines = Continent-Ocean Boundary (COB). We attribute the patchy magnetic pattern to subaerial lava extrusion (e.g., Bott, 1983), interacting with the topography of pre-existing flows, and being further complicated by erosion until the ridge subsided below the wave base.

Lundin & Dore
http://www.mantleplumes.org/Iceland2.html

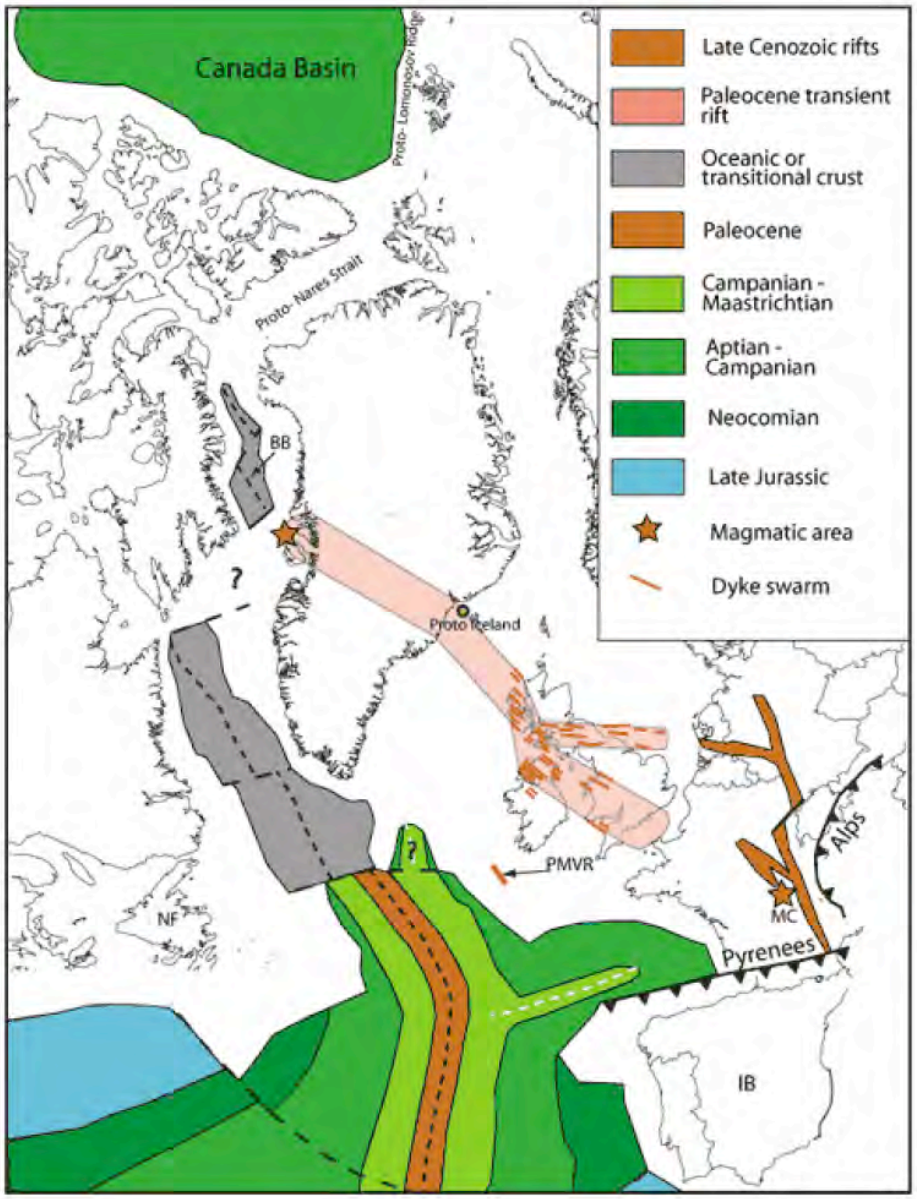

Figure 3. Plate reconstruction to 60 Ma (Trond Torsvik, pers. com. 2003) with simplified seafloor. The main dike trend in the British Volcanic Province schematically shown to extend to the West Greenland magmatic area, is invoked to utilize a zone of weak extension. The Late Cenozoic European rift system (from Ziegler, 1992) is included in order to illustrate a more evolved stage extension, also related to compression in the Pyrenees and the Alps. NF: Newfoundland, BB: Baffin Bay, IB: Iberia

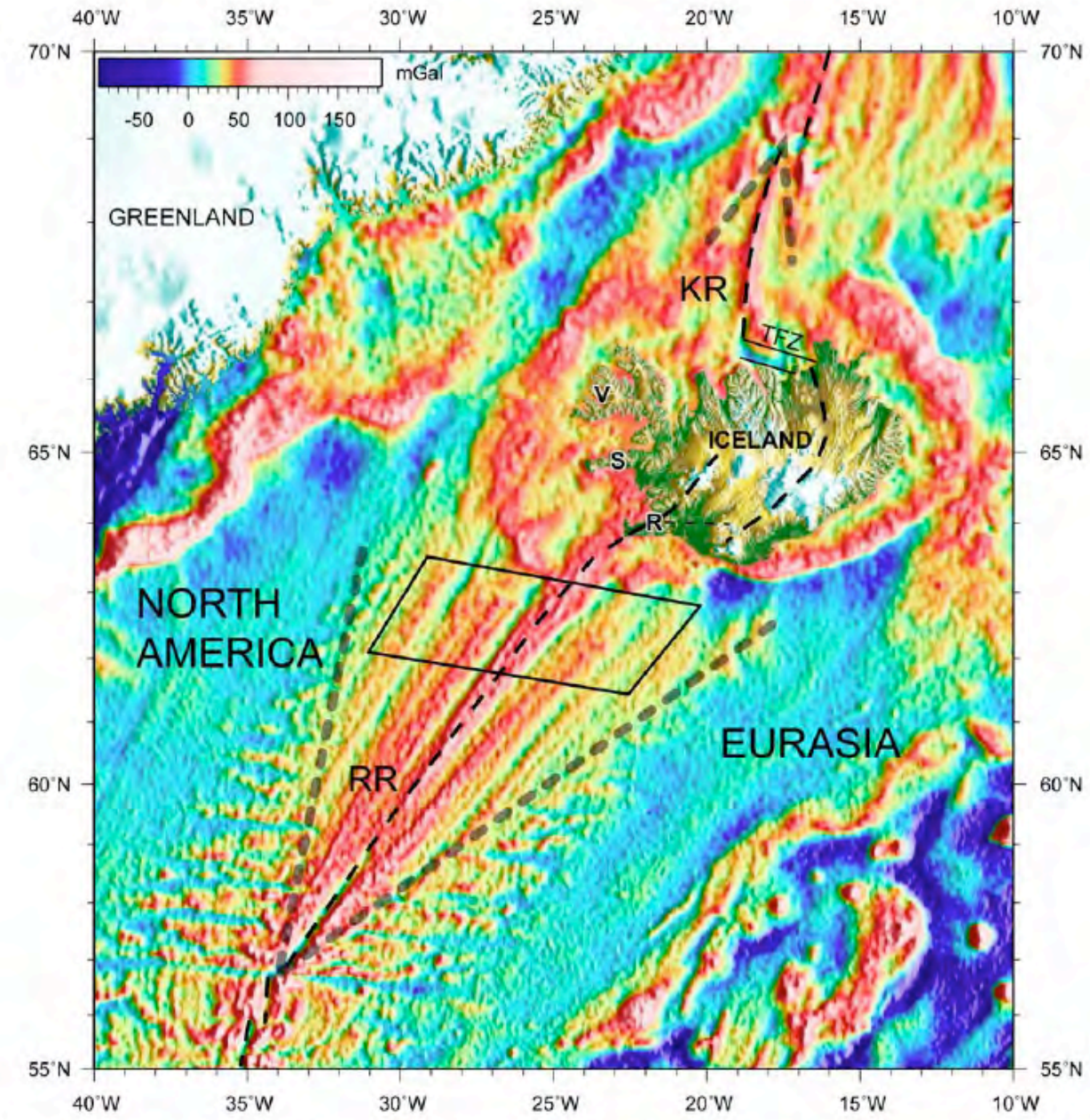

Figure 1. Satellite gravity and tectonic boundaries near Iceland [*Sandwell and Smith*, 2009] with gridded land topography superimposed. Heavy black dashes show Reykjanes Ridge (RR), Kolbeinsey Ridge (KR), and their extensions through Iceland. The VSRs we reinterpret here are the ridges and troughs slightly oblique to the Reykjanes Ridge axis enclosed by the southward pointing gray dashed V. Box shows location of profiles 16–25. TFZ, Tjornes Fracture Zone; V, Vestfirdir; S, Snæfellsnes; R, Reykjanes Peninsula.

Hey et al 2010

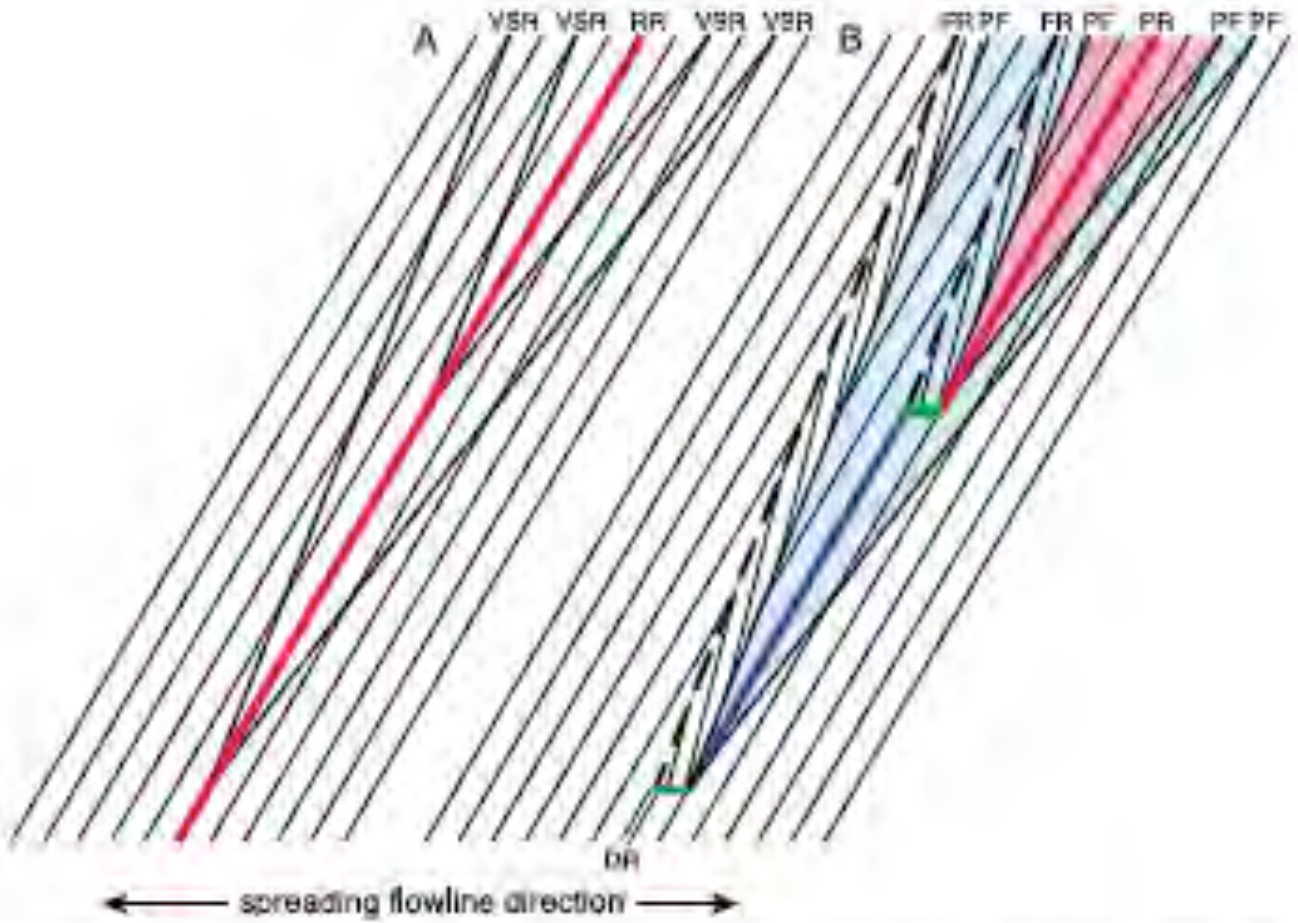

Figure 2. Alternative models for V-shaped seafloor structures, modified for oblique spreading. (a) Vogt-type variable mantle flux models [*Vogt*, 1971] produce V-shaped ridges (VSRs) and isochrons (light lines parallel to Reykjanes Ridge, RR), symmetric about the axis (red) when measured along flow lines (horizontal). (b) Propagating rift model (with ridge offsets exaggerated for clarity) produces asymmetric accretion and asymmetric V-shaped wakes. Red shaded area shows lithosphere bounded by pseudofaults (PF) created on the most recent (red) propagating rift (PR), which also produces a zone of transferred lithosphere (with rotated isochrons) and a failed rift (dashed) [*Hey*, 1977; *Hey et al.*, 1986, 1989]. Blue shaded area shows lithosphere created on previous (blue) PR axis, which is also replacing an earlier propagator (parallel black lines, DR). Note asymmetric location of youngest PR axis relative to oldest scarps and isochrons.

Hey et al 2010

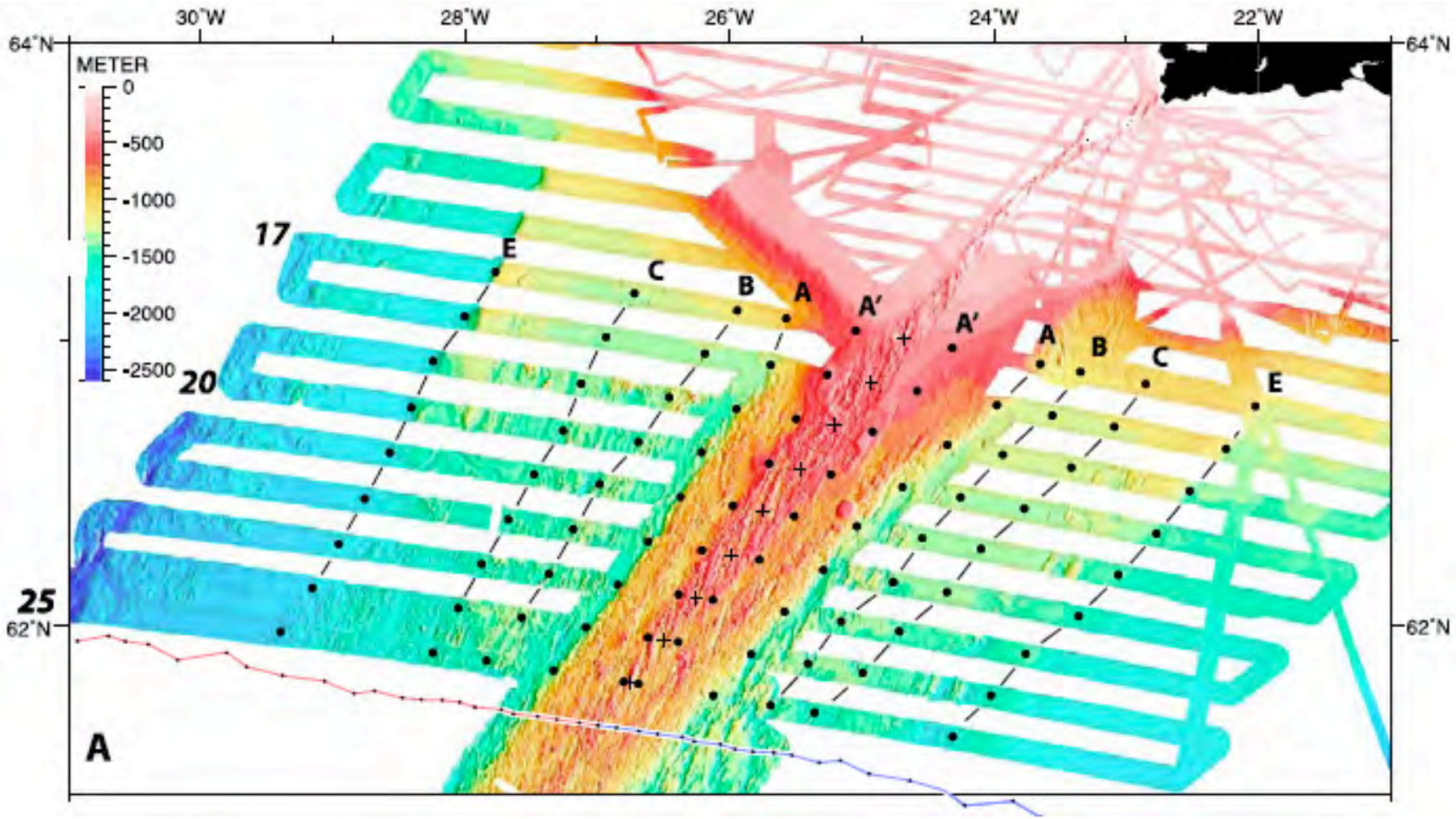

Hey et al 2010

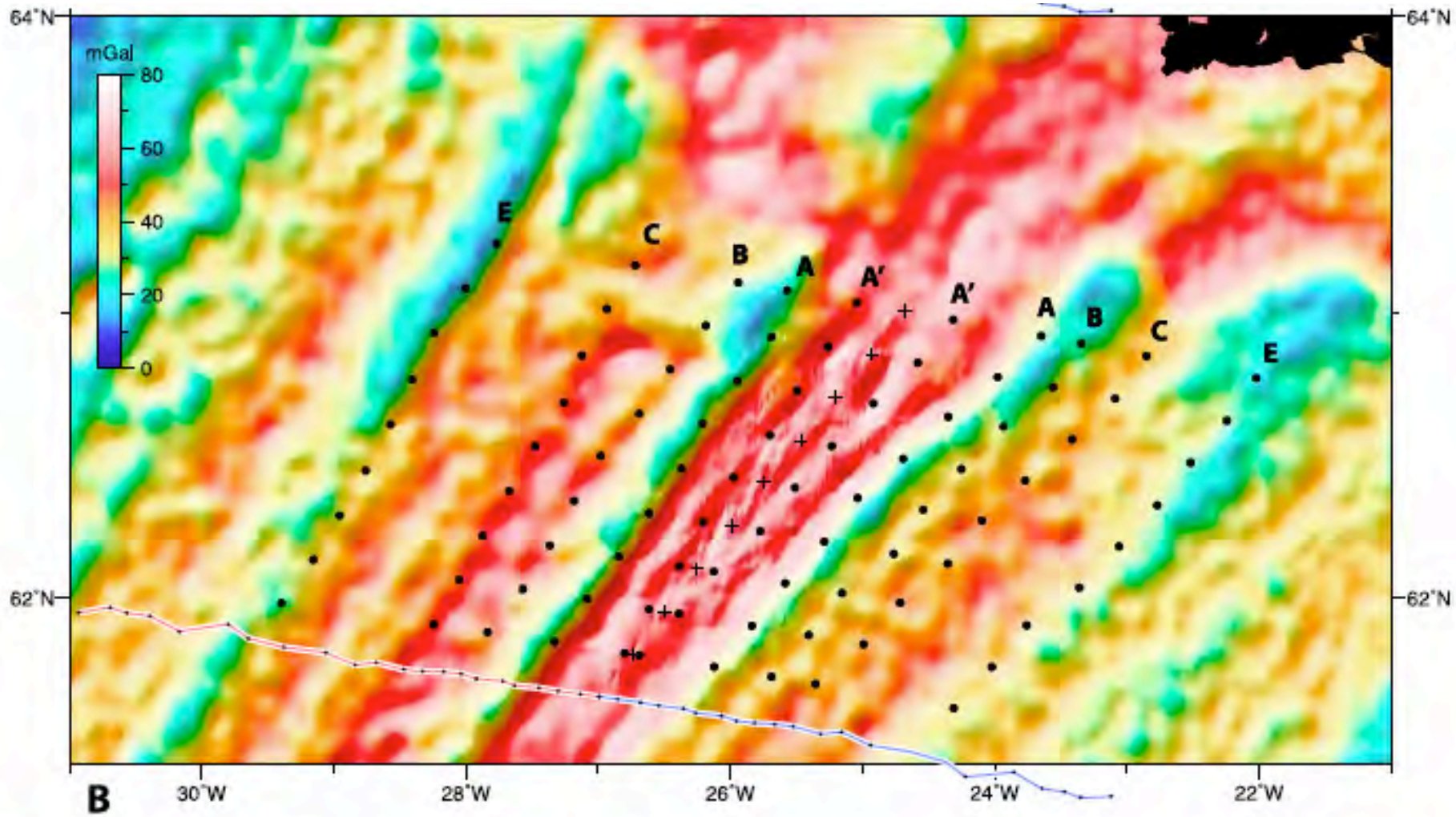

Figure 3. VSR asymmetry shown by (a) compiled multibeam bathymetry data and (b) satellite-derived gravity [*Sandwell and Smith*, 2009] combined with new axial mosaic shipboard gravity, illuminated from the southeast. The dots are the ridge jump boundaries (pseudofault wakes) used in our magnetic anomaly models (Figure 7) to fit the observed seafloor spreading asymmetry and make the conjugate scarps the same ages. Only the A and E scarps follow *Vogt*'s [1971] original terminology. Crosses show simplified seafloor spreading axis; new Seabeam track lines (numbered) are generally good approximations to the revised North America–Eurasia spreading flow lines [*Merkouriev and DeMets*, 2008] shown below our southernmost profile 25, except on the outer parts of our profiles past the E scarps. The E scarps could be interpreted differently south of profile 20, where the main gravity anomaly high shifts closer to the axis.

Hey et al 2010

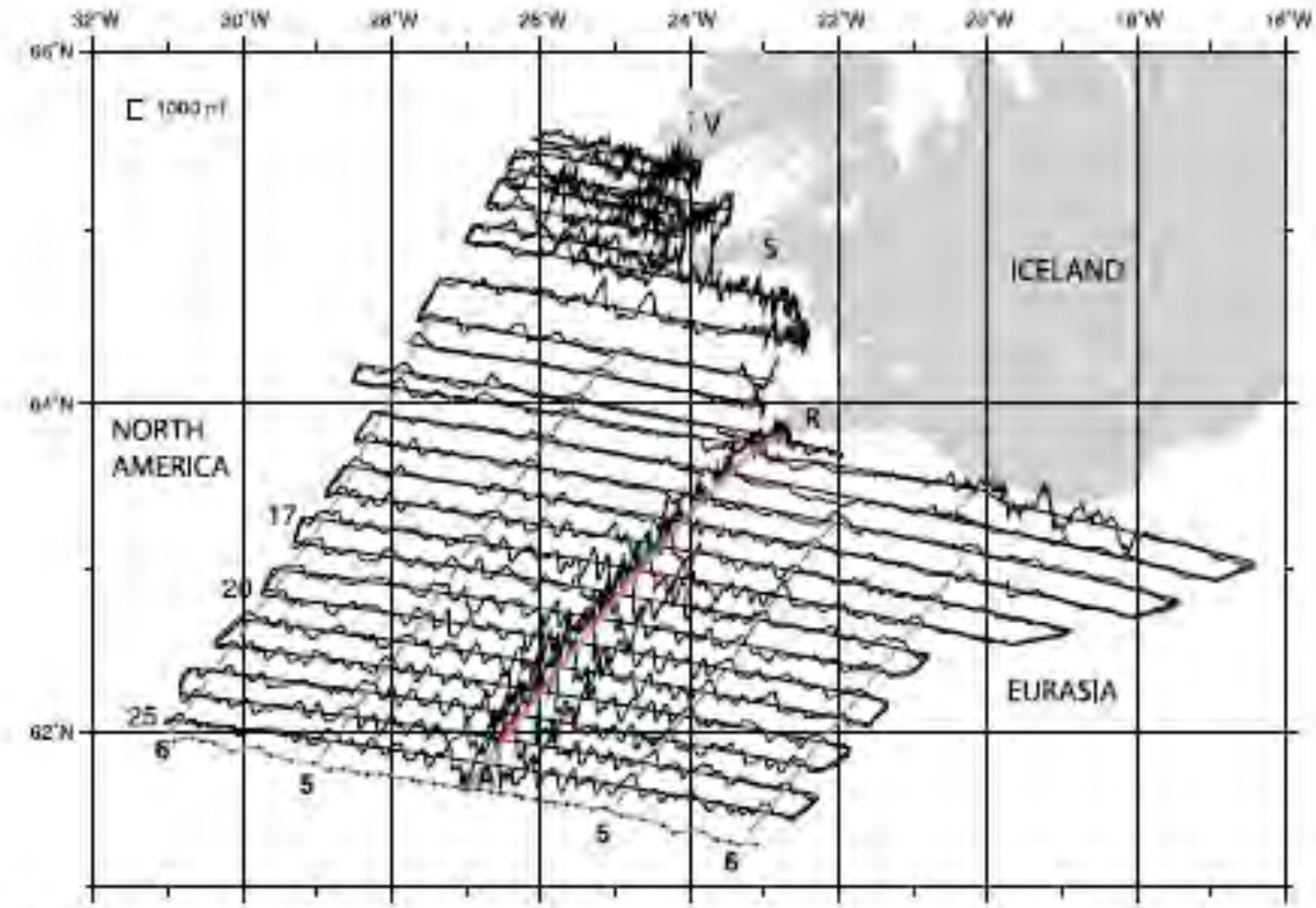

Figure 6. New marine magnetic anomaly data projected onto 010°, essentially perpendicular to track, which demonstrate asymmetric seafloor spreading. Anomalies 5 (green dashes) and 6 (blue dashes) are identified and are always farther from the ridge axis (A, red line) on North America than Eurasia, with asymmetry increasing to the north. The outermost dots in the *Merkouriev and DeMets* [2008] flow line included below the data show the predicted positions of the beginning of anomaly 6 (19.72 Ma) if spreading had been symmetric, further demonstrating asymmetry. The spacing between anomalies 5 and 6 is also consistently (~10 km) greater on North America than Eurasia, demonstrating seafloor spreading asymmetry independent of the exact location of the present ridge axis. V, Vestfirdir; S, Snaefellsnes; R, Reykjanes Peninsula.

Hey et al 2010

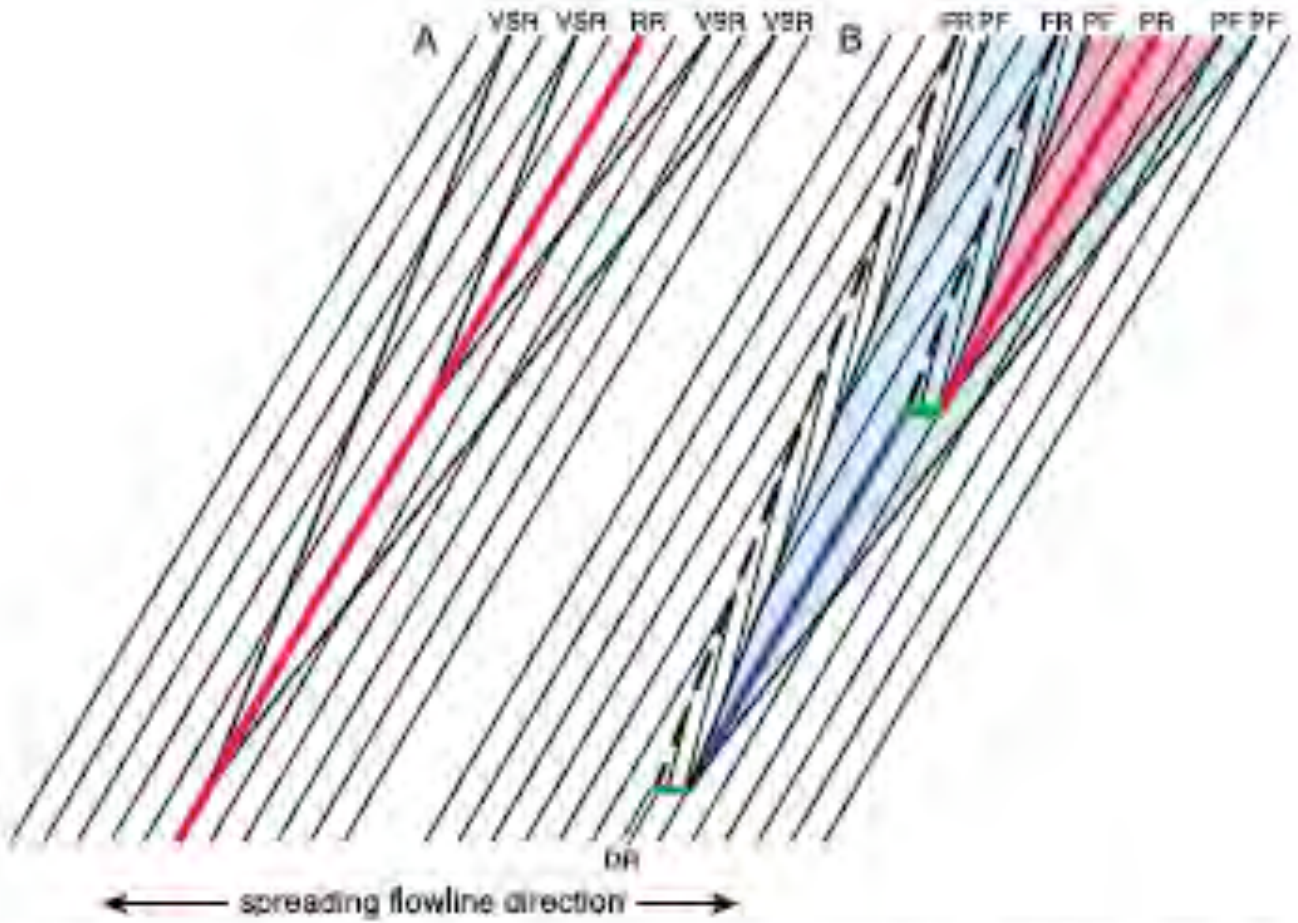

Figure 2. Alternative models for V-shaped seafloor structures, modified for oblique spreading. (a) Vogt-type variable mantle flux models [*Vogt*, 1971] produce V-shaped ridges (VSRs) and isochrons (light lines parallel to Reykjanes Ridge, RR), symmetric about the axis (red) when measured along flow lines (horizontal). (b) Propagating rift model (with ridge offsets exaggerated for clarity) produces asymmetric accretion and asymmetric V-shaped wakes. Red shaded area shows lithosphere bounded by pseudofaults (PF) created on the most recent (red) propagating rift (PR), which also produces a zone of transferred lithosphere (with rotated isochrons) and a failed rift (dashed) [*Hey*, 1977; *Hey et al.*, 1986, 1989]. Blue shaded area shows lithosphere created on previous (blue) PR axis, which is also replacing an earlier propagator (parallel black lines, DR). Note asymmetric location of youngest PR axis relative to oldest scarps and isochrons.

Hey et al 2010

Some Conclusions: Iceland

- Miocene sedimentary and volcanic units are oldest, found on western and eastern margins
- Mid-ocean ridges cross the island, creating structural topography, including grabens
- Volcanism focused in grabens
- Glaciation extended beyond present shoreline during glacial maxima
- Relative sea level varied more than eustatic sea level

Some Conclusions: Atlantic Sea Floor Spreading

- Maps of ocean magnetic stripes represent a major data compilation
- More data needs to be collected for detailed studies (See Hey et al 2010)
- Sea floor spreading began in Jurassic between North America and NW Africa
- It progressed north and south throughout the Cretaceous
- Aborted sea floor spreading between Canada and Greenland preceded sea floor spreading between Greenland and Norway

Some Conclusions: Plumes

- Plumes originally proposed (Wilson 1963)
  - Originated at mantle-core boundary
  - Fixed in the mantle
  - Persisted while plates move over plume
- Iceland interpreted as an example of a plume by Wilson, Morgan, and others
- Recent interpretations suggest a “top-down” origin for Iceland
- Debate continues at mantleplumes.org

Eyjafjallajkull Eruption: March 27, 2010

http://www.flickr.com/photos/orvaratli/4470600239/in/photostream/